A Multiscale Approach for Gas Hydrates Considering Structure, Agglomeration, and Transportability under Multiphase Flow Conditions: II. Growth Kinetic Model

Carlos Lange-Bassani, Amadeu K. Sum, Jean-Michel Herri, Rigoberto E. M. Morales, Ana Cameirão

A Multiscale Approach for Gas Hydrates Considering Structure, Agglomeration, and Transportability under Multiphase Flow Conditions: II. Growth Kinetic Model

Carlos L. Bassani[†,‡], Amadeu K. Sum[#], Jean-Michel Herri[†], Rigoberto E.M. Morales[‡*], Ana Cameirão[†*]*

[†]Mines Saint-Etienne, Univ Lyon, CNRS, UMR 5307 LGF, Centre SPIN, Departement PEG, F - 42023 Saint-Etienne France

[‡]Multiphase Flow Research Center (NUEM), Federal University of Technology – Paraná (UTFPR), Rua Deputado Heitor Alencar Furtado, 5000, Bloco N, CEP 81280-340, Curitiba/PR, Brazil

[#]Phases to Flow Laboratory, Chemical and Biological Engineering Department, Colorado School of Mines, 1500 Illinois St., Golden, CO 80401, USA

Abstract. In the second part of this series, we introduce the mathematical model for the growth kinetics of gas hydrates in oil continuous flow. Mathematical description of the capillary filling-up process is given (porosity evolution), coupled with growth phenomena already described in literature (gas absorption by the oil bulk, mass transfer particle/bulk, outer growth due to permeation). The range of closure parameters reported in literature for CH_4 hydrates is used to understand the limiting steps of crystallization, being the evolution of the porosity the controlling factor in the asymptotic trend of the gas consumed over time. Furthermore, gas absorption by the bulk, and mass transfer particle-bulk is shown to be negligible for oil-continuous flow when considering a gas that is much more soluble in oil than in water. The model is simplified for engineering purposes, giving rise to an explicit semi-empirical equation for the gas consumption rate due to hydrate formation based on two independent parameters that are experimentally regressed. A criterion for the existence of wet or dry particles (water layer covering the particles in oil-continuous flow) is proposed in means of the competition of crystal integration in the outer surface vs. water permeation through the porous hydrate.

Keywords: flow assurance, gas hydrates, growth kinetics, crystallization.

1. Introduction

Gas hydrates are crystals that form when gas and water are in contact at considerably high pressure and low temperature conditions[1]. Uncontrolled growth and agglomeration of gas hydrates is reported as the number one problem in assuring flow of oil and gas production[2]. In the first part of this series[3], we split the complex phenomena of gas hydrates formation under multiphase flow[4–

[7] (see as well videos published by Chen et al.[8]) in different size-scales that are capable of explaining their onset, growth, agglomeration and transportability in oil and gas production scenarios. In the second part, we focus on mathematical description of growth kinetics, that is, on determining the gas hydrate formation rate.

Predictive models of crystal growth kinetics can assume complex mathematical description due to the number of phenomena involved. It is therefore common to consider a limiting step of crystallization. Different limiting steps were considered in gas hydrates literature, namely: (i) absorption of gas into the continuous phase[9–13]; (ii) gas transfer particle/bulk[12]; (iii) crystal integration[9,10,14] (also called *intrinsic kinetics*); (iv) diffusion of gas through hydrate porous media[13–15]; (v) core shrinkage once gas reaches an inner core of water[13–15] (discussion about existence of water core in flowing systems is given in the first part of this series[3]); (vi) crystallization during diffusion of gas through the porous hydrate[15] (also considered as a varying diffusivity/permeation coefficient when modeling iv and vii[14]); and (vii) water permeation through the hydrate porous media, with consequent outer growth of the particle. All models need, to some extent, data regression from experiments. The models that consider less limiting steps[11,13] are of simpler regression, and therefore present better acceptance by industry. The more complex models stay theoretical and of difficult industrial application due to the high degree of freedom during regression, especially for gas-oil-water systems where phenomena (iv) to (vii) enter at play.

There is a common sense that hydrate growth kinetic models are apparatus-dependent; that is, the regressed values of one experiment cannot be extrapolated to other scenarios. Whereas stochastic behavior was often attributed to hydrate growth kinetics, we understand that different apparatus size, measured conditions and fluid properties (e.g., water or oil continuous flow, dense

or dilute flow, gas solubility in oil, multiphase flow pattern prior to onset of hydrate formation) can change the limiting steps of crystallization.

In this article, we introduce new modelling of the evolution of porosity due to filling-up of the capillaries once crystallization occurs in the capillary walls. Further coupling with phenomena (i) to (vii) gives rise to a complete (but complex) model (section 2). The range of closure parameters reported in literature for CH_4 hydrates (section 3) is used to understand the most probable limiting steps of crystallization in this case (section 4), and therefore the model is simplified to an engineering-based equation (section 5).

2. Mathematical model

A driving force is required for crystallization to initiate. For gas hydrates, this driving force is based on a difference of chemical potential of the gas component at the growing surface dissolved in liquid water and as a gas hydrate phase[16]. The chemical potential driving force is often simplified to the use of a fugacity driving force[9], which by its turn relates linearly to the concentration by using Henry's law for a dilute system[17,18]. Considering a first-order crystallization law and an activity coefficient of unity (in order to mathematically simplify the problem), the gas consumption rate due to hydrate formation comes:

$$-\frac{1}{A}\frac{dn_g}{dt}\bigg|_{hyd} = \frac{k_i}{H_w}\left(C - H_w f_{eq}\right) \tag{1}$$

where A is the growing surface, k_i is the constant of proportionality of *crystal integration*[19] (also called *intrinsic kinetics*[14] or *rate of attachment of building units*[20]), H_w is the Henry constant of gas in water (evaluated in the solubility form[17], with units of [mol/(m^{3}Pa)]; differently of the one

used by Englezos et al.[9], which is in the volatility form [Pa]), and $f_{eq} = f_{g(T,P_{eq})}$ is the gas fugacity evaluated at the gas-water-hydrate equilibrium pressure P_{eq} related to the system temperature T. This expression depends on the concentration of gas inside water C at the growing surface. The maximum concentration is saturation of gas in water, where $C = H_w f_g$, being f_g the gas fugacity at the gaseous free phase. Sometimes in literature, $H_w\left(f_g - f_{eq}\right)$ (or simply $f_g - f_{eq}$ or related subcooling $\Delta T = T - T_{eq}$) is considered as the driving force for hydrate growth. This is only true if there is no mass transfer between the gaseous free phase to the crystal growing surface (called *equilibrium mode* in Figure 1), and represents the maximum theoretical driving force. Growth kinetics is, by definition, off equilibrium; thus all mass transfer processes for the gas to reach the growing surface cause the fugacity (and associated driving force) to decrease. To correctly model the mass transfer resistances is the challenge in hydrate growth kinetics literature.

The following considerations are done in this study: (i) liquid dominated gas-oil-water flow, with oil continuous phase; (ii) at hydrates onset, both water and oil are saturated with gas; (iii) particles form over the water droplets (i.e., particles have the same size of water droplets); and (iv) agglomeration and deposition is neglected. Differently from what is usually modeled in literature, we neglect the kinetics associated to core shrinkage in the case of a shell-particle (see discussion in first part of the series[3]; mathematical proof is given later in this section). Further, the capillary walls, the outer surface of the particle and the bulk are considered at thermal equilibrium (mathematical proof in Section 1 of Supporting Material).

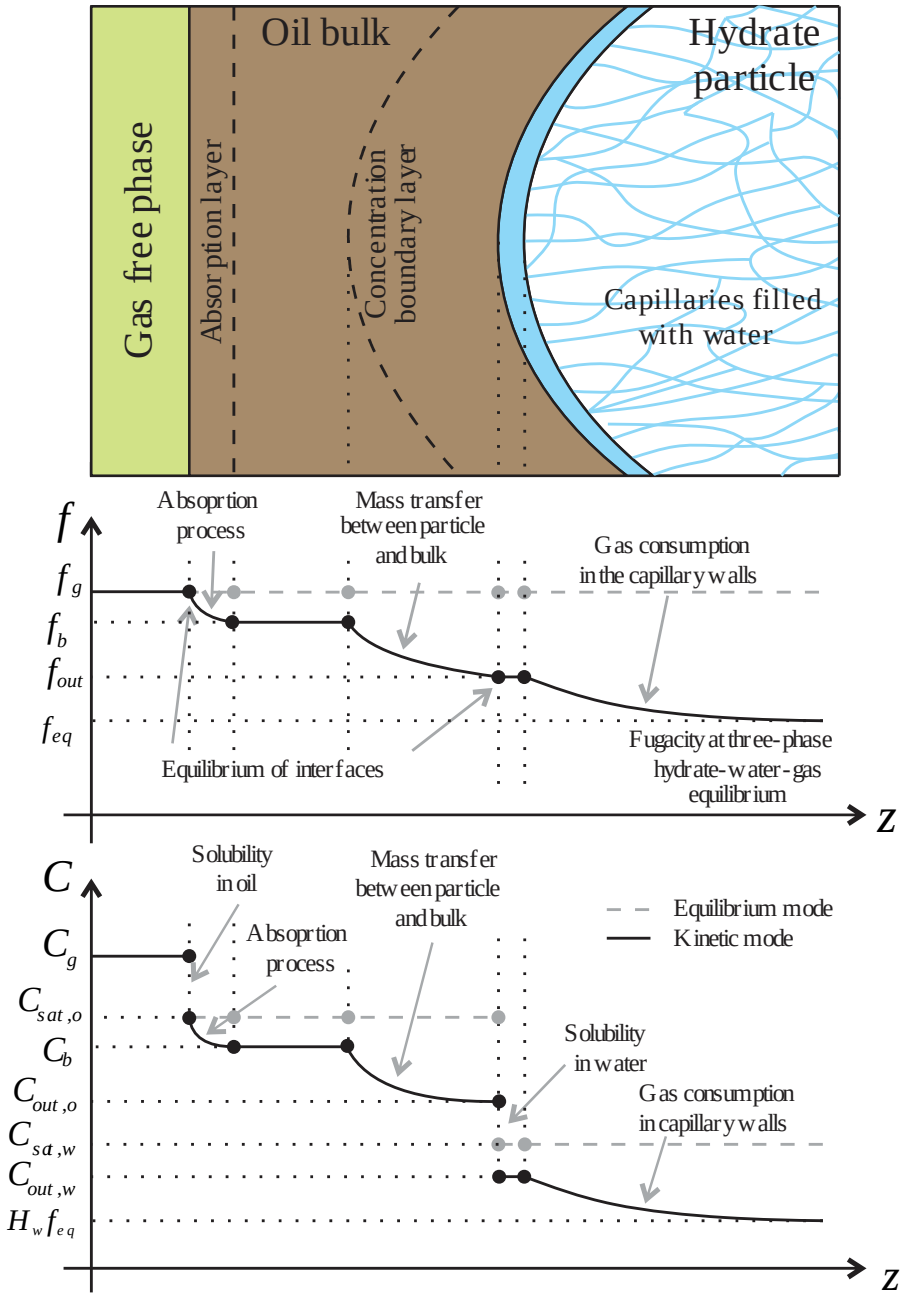

Figure 1. Fugacity and gas concentration distribution for hydrate porous particles (hydrophilic) inside oil continuous flow.

Figure 1 presents the mass transfer system and its associated fugacity and gas concentration distributions. The gas is submitted to the following processes: (a) solubilization into oil;

(ii) absorption by the oil continuous phase; (iii) distribution to all particles (the concept of bulk is used, therefore all particles receive the same concentration; discussion is given in Section 3); and (iv) mass transfer from bulk to particle. (v) Once gas arrives at the particle, it solubilizes in water (either into water accumulated at the outer surface, or into water trapped in the capillaries of the porous particle). Two distinct growing surfaces are considered: (vi) the capillary walls (gas diffuses through water entrapped in the capillary while simultaneously crystallize in its walls, causing the porous structure to seal-up in time); and (vii) the outer surface of the particle (the water that is permeated through the hydrate porous media crystallizes in the outer surface). The focus is to develop a predictive expression for the gas consumption rate due to hydrate formation given system pressure and temperature conditions, fluid properties and flow hydrodynamic conditions.

Gas concentration in the bulk

As gas is consumed at a rate $dn_g/dt\big|_{hyd}$ due to growth of all particles *i*, the oil continuous phase starts to absorb gas from the gaseous free phase at a rate $dn_g/dt\big|_{abs}$, as pointed in Figure 2. Herein, the concept of bulk is considered, i.e., the existence of part of the continuous phase where the concentration is homogeneous (constant in space). This concentration however evolves in time. Applying a gas molar balance in the bulk yields:

$$\frac{dn_b}{dt} = \left.\frac{dn_g}{dt}\right|_{abs} - \left.\frac{dn_g}{dt}\right|_{hyd} \quad \text{with} \quad \left.\frac{dn_g}{dt}\right|_{hyd} = \sum_i \left.\frac{dn_{g,i}}{dt}\right|_{hyd} \tag{2}$$

The variable of interest is the bulk concentration[9,12,21]:

$$C_b = \frac{n_b}{\forall_b} \rightarrow \frac{dn_b}{dt} = \frac{d\left(C_b \forall_b\right)}{dt} = \forall_b \frac{dC_b}{dt} + C_b \frac{d\forall_b}{dt} \approx \forall_b \frac{dC_b}{dt} \tag{3}$$

where $\forall_b$ is the bulk volume. We consider that the volume variation in time of the (oil) bulk is negligible, that is, $d\forall_b/dt \approx 0$, since oil is incompressible and is not consumed during hydrate formation. Further implications in this consideration are: (i) no trapping of the oil phase into the porous structure of gas hydrates (which could happen in the presence of surfactant additives[3]); and (ii) negligible variations of the thicknesses of the absorption gas/bulk and mass transfer particle/bulk layers.

The absorption process is modeled by a mass transfer coefficient k_{abs}, a gas-oil interfacial surface $A_{g/o}$ and a concentration gradient from the gas-oil interface to the bulk, $dn_g/dt\big|_{abs} = k_{abs} A_{g/o} \left(C_{g/o} - C_b \right)$ [9,12]. The multiphase (oil-water-gas) flow pattern is responsible for furnishing the gas-oil interfacial surface $A_{g/o}$. Although Figure 2(a) depicts slug flow pattern (intermittent passage of elongated bubbles and liquid slug, commonly found in oil and gas production[22]), the model is applicable to different flow patterns since crystallization and multiphase flow occur in different length-scales. Yet assuming the gas-oil interface at equilibrium, then the gas concentration equals saturation, $C_{g/o} = C_{sat,o} = H_o f_g$, where H_o is the Henry's constant of gas inside oil and f_g is the gas fugacity in the gaseous free phase. Inside Eq. (2):

$$\frac{dC_b}{dt} = \frac{k_{abs} A_{g/o}}{\forall_b} \left(H_o f_g - C_b \right) - \frac{1}{\forall_b} \sum_{i=1}^{n_p} \frac{dn_{g,i}}{dt}\bigg|_{hyd} \quad \text{with } C_b\big|_{t=0} = H_o f_g \tag{4}$$

where gas saturation inside the oil bulk is considered as the initial condition (the gas-oil-water mixture comes pressurized and heated from the wellbore and flows along the pipeline while gradually cools down up to reach the formation conditions). The two missing terms in Eq. (4) are: (i) the number of particles in the system n_p, herein considered constant for the sake of

simplification, but which vary due to agglomeration or breakage of particles[12,21,23–25]; and (ii) the gas consumption due to hydrate formation of each particle $dn_{g,i}/dt\big|_{hyd}$. The modeling of the latter is the focus of the next sections.

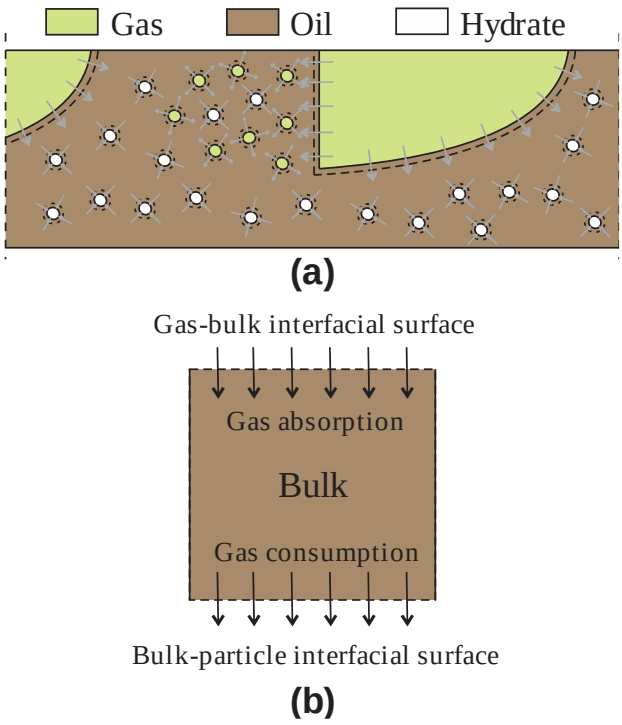

Figure 2. (a) The liquid continuous phase absorbs gas from the gaseous free phase, while the hydrate particles consume gas for crystal growth (depiction of *intermittent slug flow pattern*, but model can be used in any flow pattern since growth kinetics occur in a different length-scale compared to the flow). (b) Simplified control volume for mass balance considering a bulk region in the oil continuous phase.

Crystallization in the outer surface of the particle (outward growth)

In oil continuous flow, water is imprisoned in the hydrates porous structure (i.e., vanishing of free water flow[3]). Hydrates are usually very porous due to the high driving forces and presence of impurities in studied scenario[19,26,27]; and are hydrophilic[28] as far as the oil phase is overall nonpolar and strong surfactants at enough dosage are not present[3]. Therefore, outward growth is subjected to water availability in the outer surface. The oil-water-hydrate wetted angle $\theta_{o/w/h}$ causes a capillary-induced flow that drains the trapped water out of the porous particle. In the case of creeping flow through the porous media, friction on the capillary walls is the main resistance to flow, thus Darcy's law can be used to estimate the water permeation flow rate[29,30]:

$$Q = 4\pi r_p^2 \frac{K}{\mu_w}\left(-\frac{\Delta P_c}{L_b}\right) \text{ with } -\Delta P_c = \frac{2\sigma_{o/w}\cos\theta_{o/w/h}}{r_c} \tag{5}$$

where $L_b = r_p$ is the linear length of permeability (no capillary tortuosity comprised), herein considered equal to the particle radius; μ_w is the dynamic viscosity of water; $\sigma_{o/w}$ is the oil-water interfacial surface; and r_c is the capillary radius. The problem consists on understanding how permeability K changes over time (similar to the scale problem discussed in Chapter 2 of Civan[30]). For the sake of simplification, we consider a simple function of permeation depending on porosity, and we further model the porosity variation in time. We use the Kozeny-Carman model for a bundle of capillary cylindrical tubes[31,32], divided by 3 since only 1/3 of the capillaries are pointing in the flowing direction[29], and considering a correction factor ζ due to non-uniformities in the capillaries bundle once capillaries are connected in series or in parallel[29] (also called *interconnectivity parameter*[30]):

$$K = \frac{\zeta}{24}\frac{\varepsilon r_c^2}{\tau^2} \tag{6}$$

where ε is the porosity and τ is the capillary tortuosity. It is worth noting that the porous media models applied in literature of gas hydrates are the Kozeny original model[31], applied by Shi et al.[14]; and the Kozeny-Carman model[31,32], applied by Mori and Mochizuki[27]. The difference here is the use of coefficient $\zeta/24$ (as proposed by Dullien[29]) instead of $1/8$; and the use of τ^2 instead of τ for the Kozeny original model[14,31]. In any case, prediction of ζ is very sensitive to the porous media geometry and usually data regression is needed. Using Eq. (6) in (5), the permeation flow rate of water through the porous hydrate becomes:

$$Q = \zeta \frac{\pi}{3} \frac{r_c r_p}{\tau^2} \frac{\sigma_{o/w} \cos\theta_{o/w/h}}{\mu_w} \varepsilon \tag{7}$$

where $\varepsilon_{(t)}$ will be modeled further in this article. If all the water that arrives to the outer surface of the particle instantly crystallizes[14], then the water consumption due to hydrate formation (with related gas consumption) becomes:

$$-\frac{dn_w}{dt}\bigg|_{out}^{\max} = \frac{\rho_w}{M_w} Q \text{ and } -\frac{dn_g}{dt}\bigg|_{out}^{\max} = \frac{\rho_w}{\eta M_w} Q \tag{8}$$

where η is the hydration number following the 'stoichiometric' relation $1G + \eta H_2O \rightarrow (1+\eta) Hyd$; and ρ_w and M_w are the density and molar mass of water. This is the case of maximum hydrate formation rate in the outer surface. However, if sufficient water permeates through the hydrate shell, then water will be abundant and a crystal integration process based on the gas fugacity difference can limit outer growth. The gas consumed due to outer growth is modeled by a minimum function between permeation and crystal integration processes:

$$-\frac{dn_{g,i}}{dt}\bigg|_{out} = \min\left[\frac{\rho_w}{\eta M_w} Q \; ; \; 4\pi r_p^2 k_i \left(\frac{C_{out,o}}{H_o} - f_{eq} \right) \right] \tag{9}$$

where the fugacity in the outer surface comes from the equilibrium at the oil-water interface, $C_{out,w}/H_w = f_{out,w} = f_{out,o} = C_{out,o}/H_o$ (Figure 1). The oil phase is chosen, since $C_{out,o}$ is the concentration that plays a role in mass exchange between the particle and the bulk:

$$-\left.\frac{dn_{g,i}}{dt}\right|_{hyd} = 4\pi r_p^2 h_{m,p/b}\left(C_b - C_{out,o}\right) \rightarrow C_{out,o} = C_b - \frac{1}{4\pi r_p^2}\frac{1}{h_{m,p/b}}\left(-\left.\frac{dn_{g,i}}{dt}\right|_{hyd}\right) \tag{10}$$

where $h_{m,p/b}$ is the mass transfer coefficient between particle and bulk, and $-dn_{g,i}/dt\big|_{hyd} = -dn_{g,i}/dt\big|_{out} - n_c\, dn_{g,i}/dt\big|_{1cap}$ refers to the gas consumption due to hydrate formation in one single particle i. Substituting Eqs. (7) and (10) in (9):

$$-\left.\frac{dn_{g,i}}{dt}\right|_{out} = \min\left\{\begin{array}{l} \zeta\dfrac{\pi}{3}\dfrac{\rho_w}{\eta M_w}\dfrac{r_c r_p}{\tau^2}\dfrac{\sigma_{o/w}\cos\theta_{o/w/h}}{\mu_w}\varepsilon \quad ; \\ 4\pi r_p^2\dfrac{k_i}{H_o}\left[C_b - H_o f_{eq} - \dfrac{1}{4\pi r_p^2}\dfrac{1}{h_{m,p/b}}\left(-\left.\dfrac{dn_{g,i}}{dt}\right|_{hyd}\right)\right] \end{array}\right\} \tag{11}$$

which is an expression for the total gas consumption due to outer growth of the particle. In the Supporting Material (Section 2, Demonstration #1), it is shown how to retrieve the linear outer growth rate of the particle dr_p/dt from Eq. (11), which has application into solving the growth term of the Particles' Population Balance[9,12,21,24] and in estimating the consolidation efficiency between two particles that efficiently collides[33,34].

Crystallization in the capillary walls

The hydrate porous structure is considered entirely filled with water (hydrophilic nature[14,28]). Straight, cylindrical capillaries with an average radius of r_c are considered, valid for $r_c << L_c$,

being L_c the capillary length. As presented in Figure 3(a), gas is consumed in the capillary walls while it diffuses in z direction, being $z = 0$ at the outer surface of the particle and the positive direction of z pointing inwardly to the particle. Considering: (i) stagnant water (water actually permeates at a low velocity, i.e., creeping flow, but this is neglected for the sake of simplification); (ii) steady-state concentration profile; and (iii) Fick's law for diffusion of gas through water; then the molar balance applied to control volume of Figure 3(b) becomes:

$$-D_w \frac{d^2C}{dz^2}\pi r_c^2 dz + \frac{k_i}{H_w}\left(C - H_w f_{eq}\right)2\pi r_c dz = 0 \tag{12}$$

where C is the gas concentration inside the water trapped in the capillary, D_w is the gas diffusivity in water and H_w is the Henry's constant of gas inside water. This differential equation, Eq. (12), is very similar to the literature of gas hydrate formation in CO_2 droplets[35–38], but for steady-state. As a new feature, herein we consider the influence of the enhancement of the crystallization surface per unit volume as the capillaries decrease in radius (coming from the ratio of the crystallization surface to diffusion volume, $2\pi r_c dz / \pi r_c^2 dz = 2/r_c$ for a cylindrical capillary), which was omitted in literature. In dimensionless form, the differential equation is:

$$\frac{d^2\bar{C}}{d\bar{z}^2} - \mathrm{Ha}_c^2 \bar{C} = 0 \tag{13}$$

$$\mathrm{Ha}_c = \sqrt{\frac{2r_c k_i}{D_w H_w}} \tag{14}$$

$$\bar{z} = \frac{z}{r_c} \tag{15}$$

$$\bar{C} = \frac{C - H_w f_{eq}}{H_w f_{eq}} \tag{16}$$

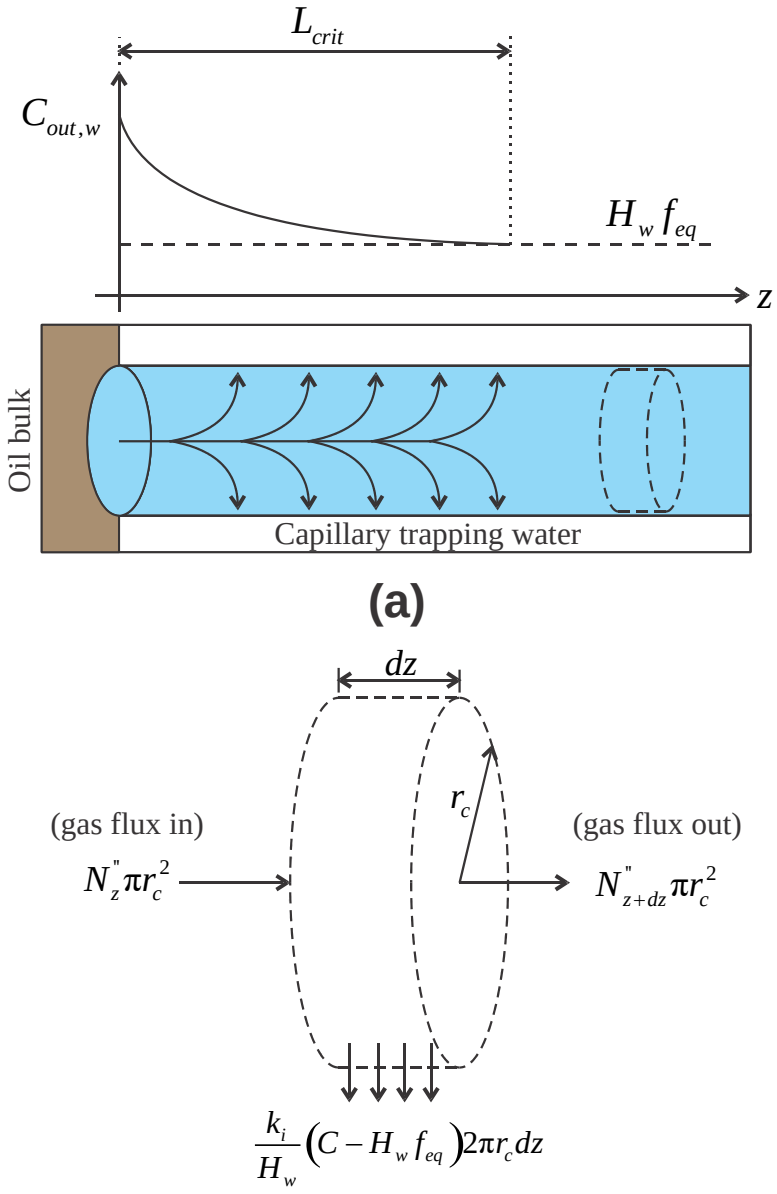

Figure 3. (a) Gas diffuses through water inside the capillaries of the hydrate porous structure while it is consumed for crystallization in the capillary walls, causing a gas concentration distribution along the capillary. (b) Control volume for gas molar balance of Eq. (12).

where the Hatta number of the capillary Ha_c expresses competition between crystal integration in the capillary walls and gas diffusion through water along the capillary (the same Hatta number analysis appears in Englezos et al.[9], but applied to a different problem geometry; the Hatta number is similar to Damköhler number; for the capillaries we use Hatta, whereas Damköhler will be used in the agglomeration analysis of section 5). The dimensionless axial position is relative to the capillary radius, Eq. (15); whereas the dimensionless gas concentration is the driving force relative to the three-phase gas-water-hydrate equilibrium condition. This dimensionless concentration $(C - H_w f_{eq})/(H_w f_{eq}) \geq 0$ is called supersaturation (not to be confused with the other definition of supersaturation also often applied in literature, $C/(H_w f_{eq}) \geq 1$[19]).

The first boundary condition at $z = 0$ is a known concentration at the outer surface of the particle (inside water phase). In dimensionless form:

$$C\big|_{z=0} = C_{out,w} \rightarrow \bar{C}\big|_{\bar{z}=0} = \frac{C_{out,w} - H_w f_{eq}}{H_w f_{eq}} = \bar{C}_{out,w} \tag{17}$$

which is estimated by considering the dissolution of gas passing from oil to water, with equilibrium at its interface:

$$f_{out,o} = f_{out,w} \rightarrow \frac{C_{out,o}}{H_o} = \frac{C_{out,w}}{H_w} \rightarrow C_{out,w} = \frac{H_w}{H_o} C_{out,o} = \frac{H_w}{H_o}\left[C_b - \frac{1}{4\pi r_p^2} \frac{1}{h_{m,p/b}} \left(-\frac{dn_{g,i}}{dt}\bigg|_{hyd} \right) \right] \tag{18}$$

where $C_{out,o}$ is the concentration used in the mass transfer process between the particle and the bulk, estimated through Eq. (10). Due to the implicit nature of this boundary condition on $(-dn_{g,i}/dt|_{hyd})$, a quasi-steady state approach is used; that is, $-dn_{g,i}/dt|_{hyd}$ is considered nearly constant in one time step of the solution and then updated for the next one.

The second boundary condition is taken as an existent water core that will completely consume the remaining gas in the inner surface of the particle in the case of inner growth (core shrinkage) at $z = L_c$:

$$-\pi r_c^2 D_w \left.\frac{dC}{dz}\right|_{z=L_c} = -\pi r_c^2 \frac{k_i}{H_w}\left(C\big|_{z=L_c} - H_w f_{eq}\right) \rightarrow \left.\frac{d\bar{C}}{d\bar{z}}\right|_{\bar{z}=\bar{z}_c} = \frac{r_c k_i}{D_w H_w}\bar{C}\big|_{\bar{z}=\bar{L}_c} = \frac{\mathrm{Ha_c}^2}{2}\bar{C}\big|_{\bar{z}=\bar{L}_c} \tag{19}$$

The inner core is herein considered to exist to further prove that it is very unlikely that gas can penetrate considerable distances up to reach the water core at enough concentrations that would promote core shrinkage. The capillary length, in the case of water core existence, is described by the capillary tortuosity multiplied by the shell width, $L_c = \tau\left(r_p - r_{in}\right)$, being r_{in} the inner and outer radius of the shelled particle. The dimensionless capillary length is $\bar{L}_c = L_c / r_c$. The gas concentration at the inner core is considered equal to the arriving gas concentration from the gas diffusion in water, $C_{in} \approx C\big|_{z=L_c}$, since gas diffusion through solid is negligible at the given system temperatures[39,40]. This boundary condition naturally converges for the non-existence of inner growth in the case of large capillary lengths, where gas consumption is such that no driving force exists at the end of the capillary:

$$\text{If } \tau\left(r_p - r_{in}\right) >> r_c \text{ then } \bar{z} \rightarrow \infty, \text{ with } \bar{C}\big|_{\bar{z}\rightarrow\infty} \rightarrow 0 \text{ and } \left.\frac{d\bar{C}}{d\bar{z}}\right|_{\bar{z}\rightarrow\infty} \rightarrow 0 \tag{20}$$

Solving Eq. (13) with boundary conditions of Eqs. (17) and (19) yields:

$$\bar{C}_{(\bar{z})} = \bar{C}_{out,w}\left[\cosh\left(\mathrm{Ha_c}\bar{z}\right) + \frac{\frac{\mathrm{Ha_c}}{2}\cosh\left(\mathrm{Ha_c}\bar{L}_c\right) - \sinh\left(\mathrm{Ha_c}\bar{L}_c\right)}{\cosh\left(\mathrm{Ha_c}\bar{L}_c\right) - \frac{\mathrm{Ha_c}}{2}\sinh\left(\mathrm{Ha_c}\bar{L}_c\right)}\sinh\left(\mathrm{Ha_c}\bar{z}\right)\right] \tag{21}$$

Knowing that $\lim_{x\to\infty}\sinh(x)=\lim_{x\to\infty}\cosh(x)$ and that the hyperbolic sine and cosine converge for considerably small arguments (≈ 2.5); then Eq. (21) can be rewritten as:

$$\bar{C}_{(\bar{z})}=\bar{C}_{out,w}\left[\cosh\left(\mathrm{Ha_c}\bar{z}\right)-\sinh\left(\mathrm{Ha_c}\bar{z}\right)\right] \text{ for } \mathrm{Ha_c}\bar{L}_c\geq 2.5 \quad (22)$$

Notice that Eq. (22) is the solution of Eq. (13) when considering that no driving force exists in the inner surface of the particle, i.e., boundary condition of Eq. (20). Therefore, criterion $\mathrm{Ha_c}\bar{L}_c\geq 2.5$ can be used to understand if ever inner growth is important or not. Considering the range of values of Table 1 for CH_4 hydrates, then $\mathrm{Ha_c}=0.01-2.7$, which gives a critical penetration length of gas inside the capillaries of $\bar{L}_{c,crit}=0.9-168$ (such a variation comes from the high degree of incompatibility in literature for k_i estimation; further discussion is given in Sections 3 and 4). For capillary lengths higher than the critical one, all gas is consumed in the capillaries and inner growth will not happen even if the water core exists. Considering, e.g., $r_c=0.5\,\mu\mathrm{m}$, then $L_{c,crit}=0.5-83.2\,\mu\mathrm{m}$. With a capillary tortuosity of $\tau\approx 5$, the maximum shell width for inner growth to be important ranges from $L_{c,crit}=0.1-16.6\,\mu\mathrm{m}$, which is negligible for the length scale of particles of this study (~ 1 mm; see Figure 6). Actually, if ever the water core exists, *the range of widths where core shrinkage is important would cause very unstable shells, which would split due to flow turbulence and rearrange into a porous structure*[41]. From now on in this article, we consider mathematically proved that core shrinkage is not an important phenomenon for *flowing* systems in the means of the range of closure parameters available in literature (at least for the CH_4 case).

By substituting Eqs. (18) and (22) in (1), by recognizing that $-dn_{g,i}/dt\big|_{hyd}=-dn_{g,i}/dt\big|_{out}-n_c\,dn_{g,i}/dt\big|_{1cap}$ and by multiplying by the number of capillaries per

particle n_c and the number of particles in the system n_p, the total gas consumption due to crystallization in the capillary walls (of all capillaries in all particles) is (see Section 2, Demonstration #2 of Supporting Material):

$$-\left.\frac{dn_g}{dt}\right|_{cap} = n_p n_c \frac{\pi r_c^{3/2}}{(1+\omega)} \sqrt{2H_w D_w k_i} \left[\frac{C_b}{H_o} - f_{eq} - \frac{1}{4\pi r_p^2} \frac{1}{H_w h_{m,p/b}} \left(-\left.\frac{dn_{g,i}}{dt}\right|_{out} \right) \right] \tag{23}$$

$$\omega = \frac{n_c}{h_{m,p/b}} \frac{H_w}{H_o} \frac{r_c^{3/2}}{4r_p^2} \sqrt{\frac{2D_w k_i}{H_w}} \tag{24}$$

where ω represents how the resistance due to mass transfer between the particle and the bulk affects consumption in the capillary walls. For $h_{m,p/b} \to \infty \ \therefore \ \omega \to 0$, this resistance is negligible; and for $h_{m,p/b} \to 0 \ \therefore \ (1+\omega) \to \omega$, mass transfer between particle and bulk is predominant. Yet, the last term inside parenthesis couples outer growth with crystallization in the capillary walls, that is, gas consumption in outer growth reduces gas availability to diffuse into the capillaries. In Eq. (23), both the number of capillaries and the number of particles evolve in time and represent the coupling between the scales of the capillary $(\sim 0.1-1\ \mu\text{m})$, the particle $(\sim 0.5-5\ \text{mm})$ and the pipeline diameter $(\sim 0.1-0.5\ \text{m})$ in order to find the total amount of gas consumption per unit volume of the pipeline. The evolution of the number of capillaries will be treated in the next section, whereas the number of particles is fixed for this study (hypothesis of no agglomeration).

Porosity evolution in time

Whereas a constant averaged capillary radius is considered throughout the entire crystallization process, the evolution of the number of capillaries per particle in time is taken into consideration. Herein, a capillary is counted only if its extremity is open to the outer surface, i.e., to the oil

continuous phase. Otherwise, gas diffusion through the solid hydrate matrix would be necessary for the gas to get in contact with water (which is negligible for the low temperatures where hydrates form[39,40]). The capillaries fill-up in time due to crystallization in their walls, but new capillaries can as well be formed due to tensioning and cracking of the crystalline structure (particles are deformable). A simplified population balance of the number of capillaries per particle is stated as:

$$\frac{dn_c}{dt} = B_c - D_c \text{ with } n_c\big|_{t=0} = n_{c,in} \tag{25}$$

where B_c is the birth rate of capillaries, D_c is the death rate of capillaries and $n_{c,in}$ is the initial number of capillaries. The capillaries are considered dead (closed) once $r_{c(t,z)} \to 0$ for any z. The death ratio of capillaries is defined as the time required for the most critical z position of the capillary to close up, which occurs at $z = 0$ (larger driving force). In this case, the driving force comes from the boundary condition, Eq. (17). Yet relating the gas consumption rate to the volume of hydrate formed, then the maximum constriction rate of a capillary is (see Section 2, Demonstration #3 of Supporting Material):

$$-\left.\frac{dr_c}{dt}\right|_{z=0} = (\eta+1)\frac{M_h}{\rho_h}\frac{k_i}{H_w}\left(C_{out,w} - H_w f_{eq}\right) = (\eta+1)\frac{M_h}{\rho_h}\frac{k_i}{H_w}H_w f_{eq}\bar{C}_{out,w} \approx cte \tag{26}$$

considered quasi-static, that is, $C_{out,w}$ varies slightly between two consecutive time steps, thus can be considered as constant and updated from step to step. By integrating from the initial capillary radius up to zero (total closing) and from time zero to the time the capillary takes to close t_{close}:

$$t_{close} = \frac{1}{\left(C_{out,w} - H_w f_{eq}\right)(\eta+1)}\frac{\rho_h}{M_h}\frac{H_w}{k_i}r_{c,in} \tag{27}$$

where $r_{c,in}$ is the initial size of the capillary, whose notation can be simplified to the averaged capillary radius r_c. From Eq. (27), the time a capillary takes to close is directly proportional to its initial size and inversely proportional to the crystal integration rate and driving force. Considering a monodispersed distribution of capillaries (i.e., all capillaries have the same size), then n_c identic capillaries close at the same time t_{close}, leading to the death rate:

$$D_c = \frac{n_c}{t_{close}} \tag{28}$$

Whereas death rate is estimated through mass transfer in the capillary, the birth rate of capillaries is yet an open question in this study. Assuming that the particle is highly deformable, flow oscillations squeeze water from the 'sponge' promoting internal tensions with micro-cracking of new capillaries (Figure 4(a)). This birth rate should then be related to the mixture flow rate. Another phenomenon is the filling-up process of the capillaries that squeeze out part of the trapped water, since the volumetric growth of hydrate is higher than the volumetric consumption of water[40]. If the capillaries fill-up homogeneously, then no internal tensions would happen. However, the filling-up process occurs from the outside to the inside of the particle (as shown Figure 4(b) due to higher driving forces near the outer surface of the particle), therefore trapping the water. Thus, a certain level of pressurization occurs (since water is incompressible), creating internal tensions and micro-cracking the structure. The just blocked capillaries then reopen (or new capillaries can be formed as well). In this case, it is fair to consider a birth rate proportional to the death rate, since the higher the filling-up rate of the capillaries, the higher the internal tensions created due to water squeezing:

$$B_c \propto D_c \rightarrow B_c = \lambda D_c = \lambda \frac{n_c}{t_{close}} \tag{29}$$

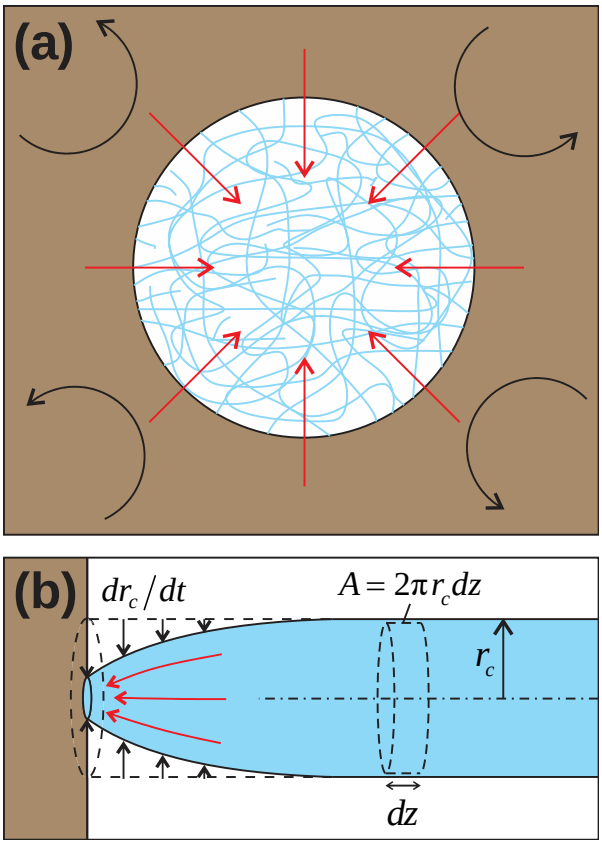

Figure 4. Birth of capillaries occur due to micro-cracking of the crystalline structure due to: (a) flow oscillations with consequent particle squeezing; and (b) squeezing of New capillaries (or reopening of already closed capillaries) occur due to micro-cracking of the crystalline structure water due to crystallization (hydrates occupy more volume than the consumed water).

where λ represents the birth-to-death ratio of capillaries. A value in the range of $0 < \lambda < 1$ shall be adopted, where: (i) $\lambda = 0$ represents no birth of capillaries, that is, all the capillaries would definitively close during time step t_{close}; (ii) $\lambda = 1$ represents that the same amount of capillaries that close will open, and no average filling-up of capillary would happen over time, with no mass transfer limitation; and (iii) $\lambda > 1$ would represents a higher quantity of capillaries being created than the ones being filled-up, which has no physical meaning if considering that the filling-up

process generates the internal tensions for the birth of capillaries. Actually, when evaluating the ratio between the time hydrates take to form (~ 30 min to 2 h[42]) and that capillaries take to close (~ 30 ms to 30 s; Eq. (27) with values of Table 1), the value of λ needs to be slightly lower than unity in order to explain the experimental results of literature. Interpretation of this birth-to-death ratio is done as follows: $1-\lambda \approx 1/100$ means that at each 100 capillaries that are filled-up, 99 capillaries are created (or reopened) due to the internal tensions and consequent micro-cracking of the particle structure. Therefore, only 1 out of 100 capillaries is, in average, filled-up during the time lapse t_{close}.

Solving Eq. (25) and using Eqs. (27) to (29), the evolution of the number of capillaries per particle becomes:

$$n_c = n_{c,in} \exp\left[-(1-\lambda)(\eta+1)\left(C_{out,w} - H_w f_{eq}\right)\frac{M_h}{\rho_h}\frac{k_i}{r_c H_w} t \right] \tag{30}$$

being $\lim_{t\to\infty} n_c = 0$ for $0 < \lambda < 1$, i.e., the capillaries will all close given enough time, which explains the asymptote of gas hydrate formation at water conversions much lower than 100%[5,13,14,43] in means of a decrease in the active surface for crystallization up to complete blockage of contact between gas and water (that is, the remaining water stays sealed inside the hydrate porous structure). Finally, the porosity at the outer surface of the particle (i.e., the porosity that is open) is related to the number of capillaries as:

$$\varepsilon = \frac{n_c r_c^2}{4 r_p^2} \tag{31}$$

or yet $\varepsilon_{\text{in}} = n_{c,in} r_{c,in}^2 / 4 r_p^2$ for the initial surface porosity. For an average capillary radius $r_c \approx r_{c,in}$, Eq. (30) equivalent for the porosity evolution over time states:

$$\varepsilon = \varepsilon_{\text{in}} \exp\left[-(1-\lambda)(\eta+1)\left(C_{out,w} - H_w f_{eq}\right)\frac{M_h}{\rho_h}\frac{k_i}{r_c H_w} t \right] \tag{32}$$

where $C_{out,w}$ relates to the bulk concentration through Eq. (18).

Calculation of total gas consumption rate / hydrate formation rate

The total gas consumption rate is due to hydrate formation at the outer surface and at the capillary walls of all n_p particles:

$$-\left.\frac{dn_g}{dt}\right|_{hyd} = \sum_{i=1}^{n_p}\left(-\left.\frac{dn_{g,i}}{dt}\right|_{out} - \left.\frac{dn_{g,i}}{dt}\right|_{cap} \right) \tag{33}$$

Solution for the total gas consumption rate $-dn_g/dt\big|_{hyd}$ is given by Eq. (33) using: (i) the gas consumption due to outer growth, Eq. (11); (ii) the gas consumption in the capillary walls, Eq. (23); (iii) the number of open-capillaries (or porosity), Eqs. (30) and (32); and (iv) the gas concentration in the water layer at the outer surface of the particle, Eq. (18). The final expression is implicit in $-dn_g/dt\big|_{hyd}$, and therefore a quasi-static numerical solution is employed, being the implicit terms of $-dn_g/dt\big|_{hyd}$ evaluated at the last time step and updated from step to step in the solution. Further coupling with Eq. (4) for the bulk concentration is needed (via numerical integration). The final system is 2×2 (gas consumption rate and bulk concentration). Finally, the hydrate formation rate and water consumption rate (molar basis) are found through the 'stoichiometric' relation $1G + \eta H_2O \rightarrow (1+\eta)\,Hyd$:

$$\frac{dn_h}{dt} = (\eta+1)\left(-\left.\frac{dn_g}{dt}\right|_{hyd} \right) \tag{34}$$

$$-\left.\frac{dn_w}{dt}\right|_{hyd} = \eta\left(-\left.\frac{dn_g}{dt}\right|_{hyd}\right) \tag{35}$$

3. Model closure and comparison with experimental data

Total closure of such predictive model for hydrate formation is hard to achieve. In this study, we selected methane hydrates (sI) for model trend validation due to the larger availability of closure parameters. Table 1 presents the range of values found in literature. The model was regressed against an experiment in the flow loop described by Melchuna et al.[5] for deionized water, methane and Kerdane[44] (light oil with composition from C11 to C14) at medium water cut (32.25 vol%). Methane is saturated in the liquid phase (that is, there is no free gaseous phase in the flow loop). The characteristics of the flow loop and of the measured case are presented in Table 2.

Infinite sets of regressed parameters are possible due to the considerable high degrees of freedom of the model, which is common in micro-scale problems of coupled crystallization and porous media (see, e.g., Shi et al.[14]). Figure 5 compares model *vs.* experiment for the molar amount of gas consumed over time, which shows that the model is capable of predicting the asymptotic trend of gas consumption over time.

A sapphire window was inserted in the flow loop to estimate the size of water droplets prior to hydrate formation. The flow is submitted to an expansion and change of cross section geometry as it passes through the sapphire window (due to design restrictions on the sapphire window, e.g., sapphire window is not circular), which introduce uncertainties in the measured droplet size. The droplet size thus may be interpreted as an order of magnitude (droplets are in the mm-scale), but not as an exact value. Figure 6 presents photographs of the water-in-oil dispersion flow before hydrate formation and 10 s after.

A key parameter that triggers the entire crystallization process is the constant of proportionality of crystal integration k_i. In literature, k_i is experimentally regressed by using the law of Eq. (1) (or a correspondent one for driving forces on chemical potential[16], concentration[19] or molar fraction[45]); and by using a model for the mass transfer resistances in order to predict the gas concentration C at the growing surface in means of the gas fugacity $f_g(T,P)$ at the gaseous free phase. The reported values for sI methane hydrates spreads over several orders of magnitude, $k_i \approx 5.5\times10^{-12} - 1.8\times10^{-7}$ mol/(m^{2}sPa)[9,46,47]. This is mostly due to: (i) uncertainties on the determination of the active surface area of crystallization, i.e., a high number of small particles, which present a rough/porous surface; and (ii) uncertainties on the estimation of the mass transfer resistances (which is model-dependent).

The model herein presented can be used to predict k_i by considering that: (i) in the very beginning of nucleation, there is no porous structure yet, thus no permeation or crystallization in capillaries exist; (ii) the growing surface is equal to the droplets surface; and (iii) gas is saturated inside water, thus the driving force is $f_g - f_{eq}$. From Eq. (1):

$$k_i = \frac{1}{\left(4\pi n_d r_d^2\right)\left(f_g - f_{eq}\right)}\left(-\left.\frac{dn_g}{dt}\right|_{hyd,t=t_{nuc}}\right) \tag{36}$$

where $n_d = 3\forall_L \mathrm{WC}/(4\pi r_d^3)$ is the number of droplets in the system considering an average droplet size r_d, WC is the water cut (volumetric fraction of water inside oil-water mixture) and $\forall_L$ the liquid volume (water + oil). Equation (36) is valid for a homogeneously dispersed flow (i.e., low water cut and high mixture velocity[48]), where droplets are fairly round; and considers that all droplets interact equally during nucleation (concept of instantaneous nucleation[49]). From Figure 6, we see that the hypothesis of instantaneous nucleation is valid since all droplets are converted to

hydrate particles in the first 10 s of crystallization. However, the flow prior to nucleation is dense, incurring in a considerable range of droplet radius, $r_d = 0.4 - 2\ \text{mm}$ (Table 2). Using the values of Table 1 and the experimental value of $-dn_g/dt\big|_{hyd,t=t_{nuc}} \approx 1.1\times10^{-3}$ mol/s (derivative of Figure 5, being $t_{nuc} = 0$ in Figure 5) into Eq. (36), then $k_i \approx 1.6 - 8.3\times10^{-11}$ mol/(m^{2}sPa). This shows the high sensitivity of Eq. (36) to the droplet size, giving deviations in about one order of magnitude for k_i. The regressed values are in between the proposed values of Englezos et al.[9] and Shi et al.[14]. We adopted $k_i = 4.1\times10^{-11}$ mol/(m^{2}sPa) (for $r_d = 1\,\text{mm}$).

Whereas during nucleation all droplets are considered to crystallize evenly (since bulk is saturated), the same cannot be considered during growth. The flow is considerably dense and the small amount of gas contained in the small oil film in between particles is consumed during nucleation. Since no mass transfer resistances due to gas distribution inside the continuous phase is considered during modeling (concept of bulk), then only a part of the particles (the ones closer to the gas-oil interface) are crystallizing. The number of particles is then proportional to the number of droplets:

$$n_p = \alpha_p n_d = \alpha_p \frac{3}{4}\frac{\forall_L \text{WC}}{\pi r_d^3} \tag{37}$$

where $1 \le \alpha_p < 0$ is called the efficiency of particles interacting with the bulk. The value of $\alpha_p \to 1$ is achieved when the gas is distributed evenly in the oil continuous phase (that is, if a bulk exists over the entire process, as considered during the modeling). This happens if the particles do not interact among themselves, that is: (i) the flow is dilute; (ii) the distance of the farther particle to the gas-oil interface is considerably small; and (iii) the system is highly mixed. As the system increase in size (i.e., larger distances of particles to gas-oil interface) and the flow becomes dense,

interaction between particles cannot be neglected. In this case, the gas concentration will be dependent on the distance of the particle to the gas-oil interface. That is, the gas consumption by the particles closer to the gas-oil interface disturb crystallization of the farther particles, causing a uneven crystallization, where the hypothesis of bulk (a region of the continuous phase where concentration is homogeneous in space) is not valid; which gives rise to the use of parameter α_p.

From Figure 6, it is clear that the particles are larger than the droplets prior to nucleation and that the flow is dense. A possible way of diluting the flow and avoiding agglomeration is by using chemical additives (e.g., anti-agglomerants, often with surfactant properties). However, some other properties of the phases would be unknown in the presence of the said additives (e.g., k_i reference order of magnitude), therefore we did not used additives in this study. Yet, dilution in the flow loop employed would not avoid the use of α_p-parameter, since the available experimental apparatus presents long distances from gas-oil interface to the flowing volume (no free gaseous phase, thus $\alpha_p \to 0$ is expected). The introduction of a gas free phase (e.g., the flow loop of Ding et al.[6,7,50]) reduces the distance of particle to gas-oil interface, but incur in designing liquid-gas separation prior to the pumping system and gas reinjection after it. The flow loop available for this study is however not setup for such a task.

Finally, for parameters regression, we adopted the average droplet size filmed with the camera for the initial particle size, $r_d = r_p = 1\,\text{mm}$. The capillary radius is kept at $r_c = 0.5\,\mu\text{m}$ (in coherence with microscope visualization[51,52]) and the tortuosity at $\tau = 5$ (coherent with discussion given by Dullien[29]). Although an infinite set of regressed values exist, it should explain the asymptotic value of gas consumed shown in Figure 5 and its curvature. The asymptotic value is dependent on α_p and ε_{in}. In order to keep a fairly high initial porosity of hydrates[26] (> 50%), then $\alpha_p \to 0$

converges to values close to zero. The curvature of Figure 5 is dependent on the closure time-scale of a capillary, Eq. (27). This time-scale is small (since capillaries are small and crystal integration is considerably fast for any k_i parameter adopted), giving $t_{close} = 32.3\,\text{s}$ for the adopted $k_i = 4.1\times10^{-11}$ mol/(m^{2}sPa). Therefore, λ-parameter needs to assume low values (that is, cracking of a considerable number of capillaries occur at the same time that other capillaries close) in order to achieve the total time-scale of the experiment (~ 2 h), Figure 5. Regression converges to $1-\lambda = 0.019$, which means that at each 1000 capillaries that close during t_{close}, only 19 remain closed and the other ones reopen.

Table 1. Range of values and adopted ones for model closure.

Parameter	***Order of magnitude from literature***	***Adopted value***
Constant of proportionality of crystal integration[9,46,47,53] (CH_4 hydrates)	$k_i \approx 5.5\times10^{-12} - 1.8\times10^{-7}\ \frac{\text{mol}}{\text{m}^2\text{sPa}}$	$k_i = 4.1\times10^{-11}$ mol/(m^{2}sPa) [a]
Absorption coefficient[12,42]	$\frac{k_{abs}A_{g/b}}{\forall_b} \approx 5\times10^{-4} - 2\times10^{-2}\ \text{s}^{-1}$	$\frac{k_{abs}A_{g/b}}{\forall_b} = 1\times10^{-2}\ \text{s}^{-1}$ [b]
Mass transfer coefficient between particle and bulk[39]	$\text{Sh}_\text{p} = 2 + 0.6\,\text{Re}_\text{p}^{1/2}\,\text{Sc}^{1/3}$ [c]	$U_{p/b} = J$ [d]
Henry's constant of methane in water	$H_w = 1.4\times10^{-5}\exp\left[1600\left(\frac{1}{T}-\frac{1}{T^\circ}\right)\right]\ \left[\frac{\text{mol}}{\text{m}^3\text{Pa}}\right]$ [e]	$H_w \approx 2.06\times10^{-5}\ \frac{\text{mol}}{\text{m}^3\text{Pa}}$ [f]
Henry's constant of methane in Kerdane[42,54]	$1.1 - 3.5\times10^{-4}\ \frac{\text{mol}}{\text{m}^3\text{Pa}}$ [g]	$H_o \approx 2.70\times10^{-4}\ \frac{\text{mol}}{\text{m}^3\text{Pa}}$ [h]
Properties of methane sI hydrates[55,56]	$\rho_h \approx 917\,\text{kg/m}^3$; $M_h \approx 17.7\times10^{-3}\,\text{kg/mol}$; $\eta \geq 5.75$	$\eta = 6$ [i]
Kerdane properties[44]	$\rho_o \approx 815\,\text{kg/m}^3$; $\sigma_o = 0.0257$ N/m ; $\mu_o = 2\times10^{-3}$ Pa.s [j]	
Water and methane properties	Evaluated through RefProp[57], which calculates accurate methane properties[58]	
Diffusivities of methane in water and Kerdane[59]	$D_{g/w} = (1.24 - 2.35)\times10^{-9}\ \text{m}^2/\text{s}$ [k]	$D_{g/w} = 1.24\times10^{-9}\ \text{m}^2/\text{s}$ [l] $D_{g/o} \approx 10\times D_{g/w}$ [m]
Equilibrium pressure for a given system temperature	$P_{eq} = \left[8.34\times10^{-12}\exp(0.105T)\right]\times10^5$ [n]	$P_{eq} \approx 42.9\times10^5$ Pa
Gas fugacity in gaseous free phase	Methane fugacity from Refprop[57] evaluated at system pressure and temperature (P,T)	$f_g \approx 67.2\times10^5$ Pa
Gas fugacity at three-phase methane-water-hydrate equilibrium	Methane fugacity from Refprop[57] evaluated at equilibrium pressure and system temperature (P_{eq},T)	$f_{eq} \approx 39.1\times10^5$ Pa

Hydrate porosity	$\varepsilon_{\text{sup}} = 10-40\%$ for aged hydrates in permafrost[51] $\varepsilon_{\text{sup}} > 50\%$ for hydrates just formed in flowing conditions[26,60]	$\varepsilon_{in} = 60\%$
Capillary radius	$r_c = 0.1-0.5\ \mu\text{m}$ [o]	$r_c = 0.5\ \mu\text{m}$
Capillary tortuosity[29,32,61]	$\tau = 1-8$	$\tau = 5$
Interconnectivity of capillaries[29]	$\zeta = 0.001-0.02$ [p]	$\zeta = 0.02$
Oil-water interfacial tension	$\sigma_{w/o} = \lvert\sigma_w - \sigma_o\rvert$ [q]	$\sigma_{w/o} = 0.0491$ N/m
Oil-water-hydrate wetted angle (water-side)	$\theta_{o/w/h} < 90^o$ [r]	$\theta_{o/w/h} = 60^o$
Birth-to-death ratio of capillaries	$0 < \lambda < 1$, with probable $\lambda \to 1$ [s]	$1-\lambda = 0.019$
Efficiency of particles interacting with the bulk	$\alpha_p \to 1$ dilute flow, small systems $0 < \alpha_p \square\ 1$ dense flow, large systems	$\alpha_p = 0.03$ [t]

Notes: [a]Using Eq. (36) for $r_p = r_d = 1\,\text{mm}$. [b]Consistent with methane-water in batch reactor with high agitation[12]; and water-Kerdane in flow loop, 30% WC, J = 0.68 m/s[42]. [c]Correlation for forced convection over spheres. Relative velocity (slip velocity) between particle and bulk $U_{p/b}$ is unknown. Maximum is the mixture velocity, $U_{p/b} = J$. Minimum is zero, where $\text{Sh}_\text{p} = 2$ stays for stagnant liquid. With: $h_m = \text{Sh}_\text{p} D_{g/o}/(2r_p)$, $\text{Re}_\text{p} = 2\rho_o U_{p/b} r_p/\mu_o$, $\text{Sc} = \mu_o/(\rho_o D_{g/o})$. [d]Valid for highly agitated systems, turbulent flow. [e]With: $T° = 298.15\,\text{K}$. Validity: $\left(\lvert T° - T\rvert \le 20\,\text{K}\right)$[17]. [f]For 5ºC. [g]Range of values retrieved for methane in Kerdane[42] using definition of Henry's constant of Sander[17], but using fugacity instead of pressure. Fugacity is evaluated through RefProp[57]. This range was checked against methane solubility data[54] in Hexane, Decane and Dodecane for $(10 \le P \le 100)\times 10^5$ Pa, $277 \le T \le 400\,\text{K}$. [h]For Kerdane at 80 bar and 5ºC[42]. [i]Since hydrate kinetics cause less cage occupancy, then $\eta \ge 5.75$ (theoretical value for sI hydrate). [j]Newtonian behavior. Viscosity measured in rheometer for 4ºC, 1 bar. [k]For $283 \le T \le 308\,\text{K}$ and 1 bar. [l]For 283 K. [m]Assumption that diffusivity of methane in Kerdane is one order of magnitude higher than methane in water. [n]Pressure in [Pa], temperature in [K]. Regressed from CSMGem[62–65] for Methane sI hydrates. Valid for $(30 \le P_{eq} \le 100)\times 10^5$ Pa. [o]Visualized in microscope for natural gas hydrates in permafrost[51] and CH_4 hydrates formed over ice[52]. [p]Evaluated by considering serial and parallel connection non-uniformities with capillaries of one order of magnitude of difference in size, length and number (page 173 of Dullien[29]; range of values found by multiplying Eq. (4.3.9) by Eq. (4.3.10), that is, existence of both non-uniformities). [q]Antonoff rule[66], valid for immiscible fluids. [r]Hydrates are hydrophilic[14,28]. [s]Only a few capillaries actually stay closed due to squeezing of a very incompressible fluid, the water. [t]The flow loop used is large and flow is considerably dense.

Table 2. Characteristics of the experiment for methane hydrate formation in the flow loop described by Melchuna et al.[5]

Fluids	Methane / Kerdane[44] / Deionized water
Pipeline internal diameter	10.2 mm
Temperature	278 K
Pressure	80×10^5 Pa
Mixture velocity	0.68 m/s
Water cut	32.25 %
Volume of mixture inside flow loop	0.01 m^3 (10 liters)
Droplet radius before hydrates onset[a]	0.4 - 2 mm, average radius of 1 mm

[a]Estimated from flow visualization and manual data treatment with Web Plot Digitizer[67].

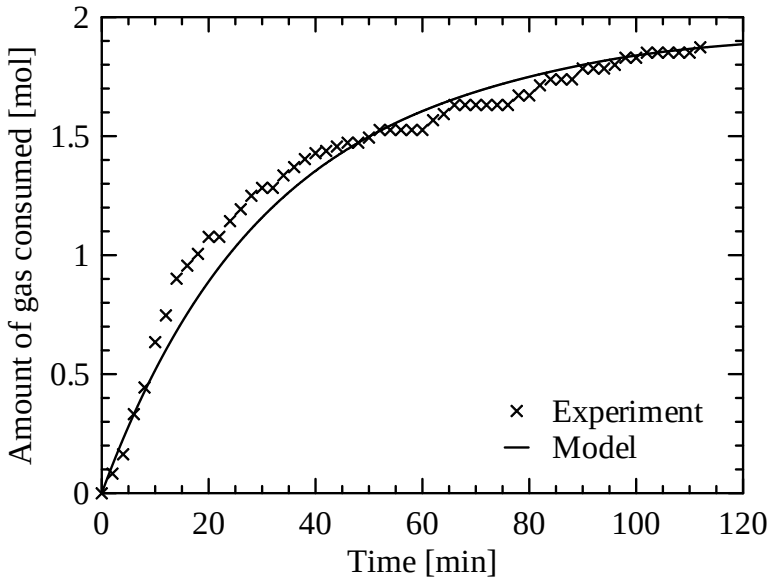

Figure 5. Model trend validation against experimental data for the molar amount of gas consumed over time. Closure properties from Table 1.

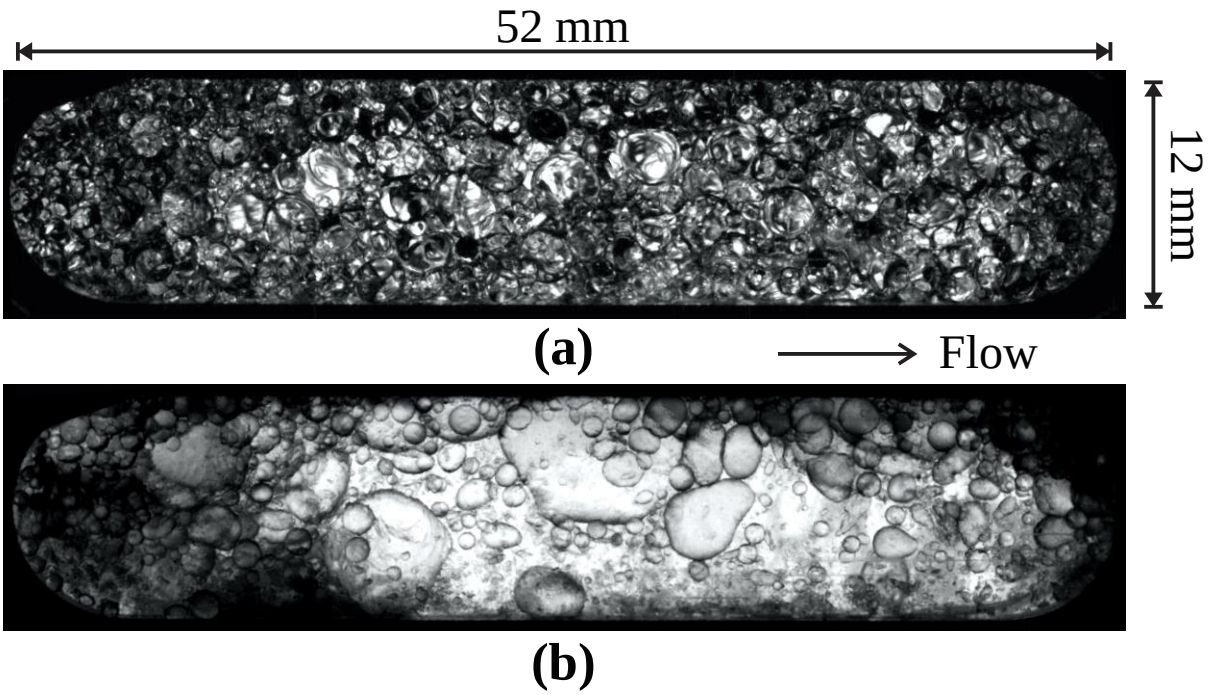

Figure 6: High-speed imaging photos of: (a) the water-in-oil emulsion flow before the onset of hydrate formation and (b) 10 s after the onset.

4. Sensitivity analysis and limiting steps of crystallization

This section is intended to understand model sensitivity to the main closure parameters and to understand the limiting steps of crystallization. The base values are given in Table 1. For mass transfer resistances in series (absorption, mass transfer, or permeation *vs.* crystal integration for outer growth), the limiting step is given as the phenomena that predicts the lower value of molar transfer rate dn_g/dt. For parallel resistances (outer growth *vs.* crystallization in capillaries), the higher value of dn_g/dt represents the limiting step. More than one phenomena can be at play if they predict the same order of magnitude for dn_g/dt. Since the phenomena evolve in time (e.g., particles seal up), then the limiting step can change.

Characteristic trends of the model

Figure 7 presents the trends captured by the model when using the base values of Table 1. The porosity (Figure 7(a), Eq. (32)), decreases exponentially in time. As the pores close, the active surface for crystallization decreases, thus decreasing the gas consumption rate (Figure 7(b)). This explains the gas consumption asymptote found in Figure 5. The slight discontinuity in the gas consumption rate (Figure 7(b), marked by a gray dashed line) is due to commutation of limiting phenomena of outer growth from crystal integration to permeation. This will be better discussed in a later subsection. The gas concentration in the bulk has a dive in the first minutes of crystallization (Figure 7(c)), due the higher amount of gas consumption and consequent depletion of the bulk (second term of the RHS of Eq. (4)). This triggers the absorption process (first term of the RHS of Eq. (4)), and the bulk starts to replenish. With the decrease of gas consumption, the gas reaches concentrations close to saturation in the bulk at the end of the crystallization process. It is worth noting that, *even if a steep dive occurs in gas concentration in oil at the beginning of crystallization (~ 25 mol/m^3), this is reflected as only a small dive in gas concentration in water (~ 1 mol/m^3) due to much higher solubilities of methane in oil than in water* $(H_o >> H_w)$, information that will be further used to discuss processes of absorption and mass transfer in the particle/bulk.

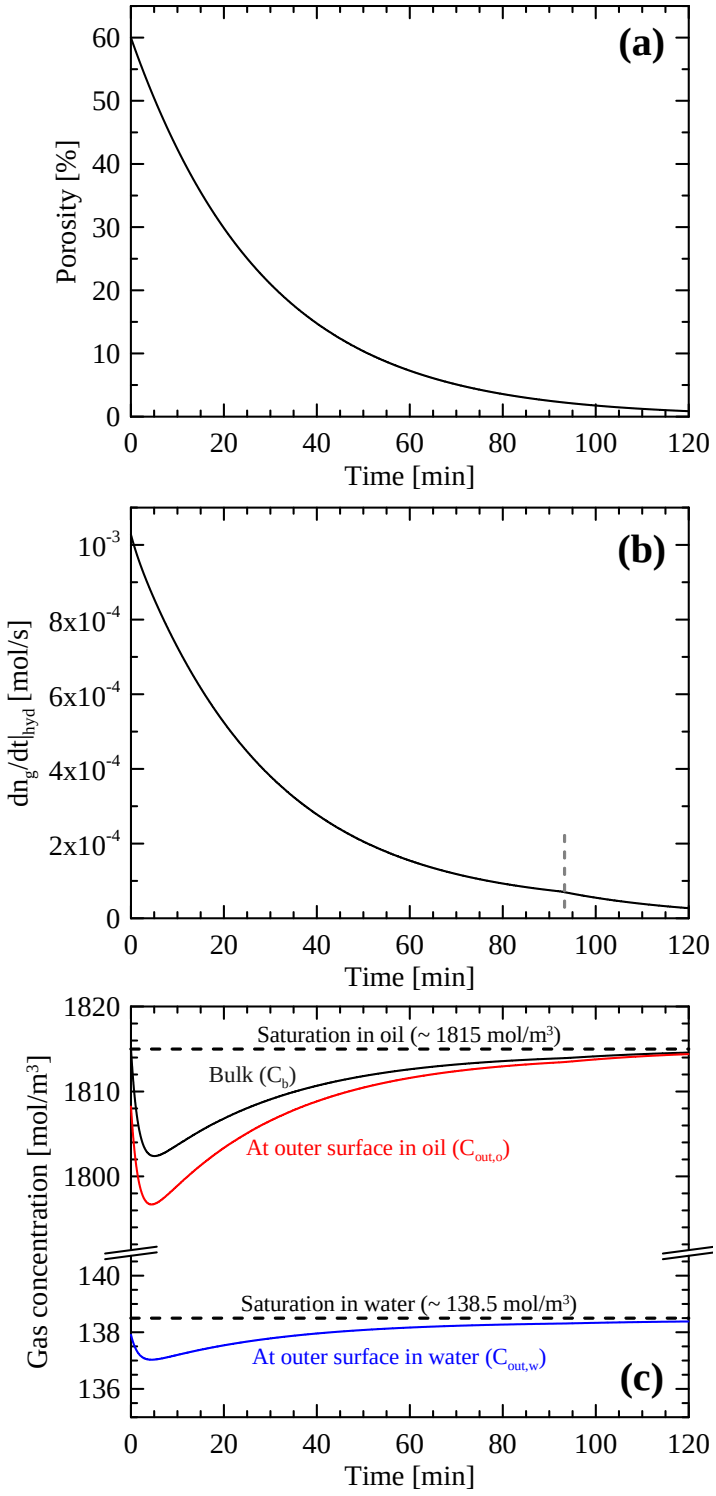

Figure 7: Trends captured by the model for: (a) porosity evolution in time; (b) gas consumption rate; and (c) gas concentration in the bulk and at the outer surface (in oil and in water). Closure properties from Table 1.

Gas absorption by the bulk: influence of gas solubility in oil and absorption coefficient

Gas absorption limits crystallization if the maximum absorption rate is in the same order of magnitude of the gas consumption rate measured in the experiment. By using the absorption law (first term of the RHS of Eq. (4)) and by recognizing that when the absorption process limits hydrate formation then gas concentration in the bulk drops to the equilibrium level, $C_b \approx H_o f_{eq}$:

(A) $\left.\frac{dn_g}{dt}\right|_{abs}^{\max} = \frac{k_{abs} A_{g/o}}{\forall_o} H_o \left(f_g - f_{eq} \right) >> \sum_{i=1}^{n_p} \left(- \left. \frac{dn_{g,i}}{dt} \right|_{hyd} \right)$, then no absorption-limited crystallization

(B) $\left.\frac{dn_g}{dt}\right|_{abs}^{\max} = \frac{k_{abs} A_{g/o}}{\forall_o} H_o \left(f_g - f_{eq} \right) \approx \sum_{i=1}^{n_p} \left(- \left. \frac{dn_{g,i}}{dt} \right|_{hyd} \right)$, then absorption-limited crystallization

Therefore, gas absorption is prone to limit crystallization when: (i) the absorption coefficient is low, for low agitated systems; (ii) the gas-oil interfacial surface per unit volume is small; and (iii) the solubility of gas inside oil is low, that is, low values of H_o. The driving force $\left(f_g - f_{eq} \right)$ appears in almost all terms of the model (excluding the permeation term for outer growth), thus its use is more complex into drawing conclusions of the limiting step. A later subsection will discuss effects of driving force.

Figure 8(a) presents the gas consumption rate estimated by the model for the extreme values of the range $5 \times 10^{-4} \le k_{abs} A_{g/b} / \forall_b \le 2 \times 10^{-2}\ \mathrm{s}^{-1}$ (specific absorption coefficient; Table 1). This parameter represents (i) and (ii) and is related to the multiphase flow pattern. For any adopted value (and considering the gas solubilities of Table 1, with $H_o \approx 10 H_w$), there is always enough gas inside oil (as already discussed from (Figure 7(c)), therefore absorption is never limiting crystallization. Although the gas concentration in water at the outer surface of the particle drops

in up to ~ 6% in the beginning of hydrate formation (Figure 8(b)), high supersaturations are kept because the bulk remains full of gas (even if mixing/absorption is low, when $k_{abs}A_{g/b}/\forall_b = 5\times10^{-4}\ \mathrm{s}^{-1}$, Figure 8(c), red line) and porosity decreases as fast as in the case of high absorption ($k_{abs}A_{g/b}/\forall_b = 10^{-2}\ \mathrm{s}^{-1}$, black line). In both cases, the gas consumption rate presents a decreasing trend (Figure 8(d)), characteristic of limitation by the sealing of capillaries.

Therefore, *absorption-limited processes are expected to be more important when the gas solubility in the continuous phase present the same order of magnitude (or lower) than the solubility of the same gas in water*. Absorption-limited crystallization is expected for, e.g.,: (i) CO_2 hydrates, being CO_2 solubility in water one order of magnitude higher than CH_4 in water ($H_{CO_2/H_2O} \approx 3.3\times10^{-4}$ mol/(m^{3}Pa)[17]); or (ii) when water is the continuous phase. Indeed, experimental evidences[5,42] report lower consumption rates for water continuous cases (high water cut systems).

Sensitivity of the model to the ratio of gas solubility in oil and water is also presented in Figure 8. When mixing/absorption is high ($k_{abs}A_{g/b}/\forall_b = 1\times10^{-2}\ \mathrm{s}^{-1}$, blue line), the bulk is quickly replenished so the gas concentration inside water at the outer surface of the particle is always kept high (maximum drop of ~ 11%; Figure 8(b)), and therefore the porosity seals up in a similar time-scale (Figure 8(c)) and the gas consumption rate is similar (Figure 8(d)). That is, even if gas solubility in water and in oil are similar ($H_o = H_w$), the absorption process does not limit hydrate formation if the system is highly mixed.

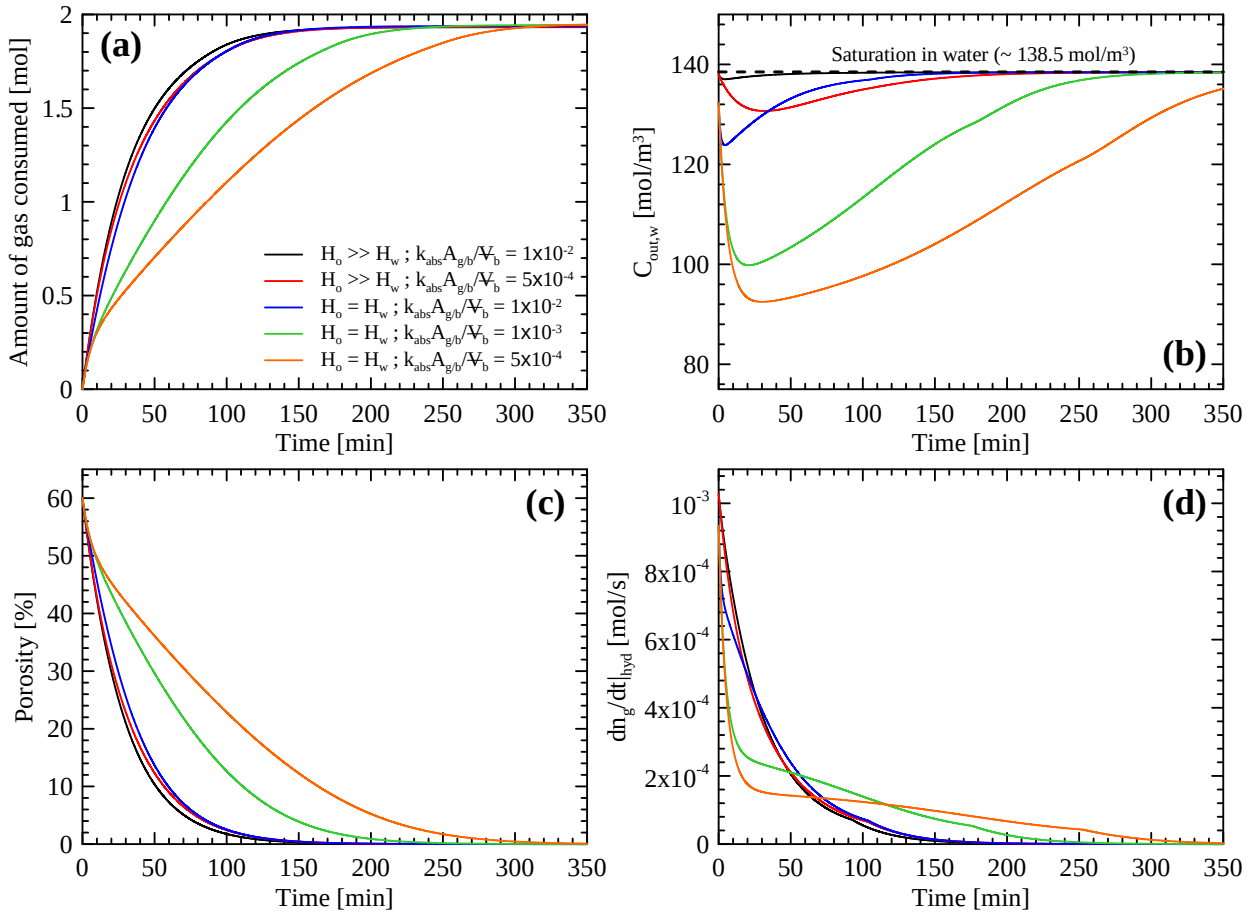

Figure 8: Sensitivity analysis of hydrate formation to specific absorption coefficient $(k_{abs}A_{g/b}/\forall_b)$ and gas solubility (Henry's constant) in oil and water (H_o, H_w) (other parameters come from Table 1). Evolution in time of: (a) gas consumed due to hydrate formation; (b) gas concentration in the outer surface of the particle inside water; (c) porosity; and (d) gas consumption rate due to hydrate formation. Absorption of gas by the bulk is capable of limiting crystallization for systems with low/medium mixing and gas solubility in oil (continuous phase) in the same order of gas solubility in water.

For lower absorption coefficients ($k_{abs}A_{g/b}/\forall_b = 5\times10^{-4}\,s^{-1}$ for low mixing, orange line; and $k_{abs}A_{g/b}/\forall_b = 1\times10^{-3}\,s^{-1}$ for medium mixing, green line), absorption starts to play a role. The gas

consumed assumes a straight line trend (Figure 8(a); the same was observed for water continuous experiments[9,12]). The gas concentration inside water in the outer surface drops in up to ~ 35% and take much longer time to be replenished towards saturation (Figure 8(b)). This reduces the driving force to seal up the capillaries, causing a slower porosity decrease in time (Figure 8(c)). As a consequence, the gas consumption rate due to hydrate formation drops to a nearly constant value in the first 20 min, and remains at this value for the next ~ 100-150 min (Figure 8(d)). Once the porosity reaches lower values, the active surface for crystallization decreases to such a point that the amount of gas consumed rate due to crystallization is lower than the maximum absorption rate, $-\left.\frac{dn_g}{dt}\right|_{hyd} < \left.\frac{dn_g}{dt}\right|_{abs}^{\max}$. Then the bulk starts to refill, furnishing higher driving forces to the outer surface of the particle (Figure 8(b)). This is when limitation start to be due to the capillaries sealing-up process, where the gas consumption rate drops (Figure 8(d); ~ 100-120 min for green line; ~ 150-200 min for orange line) and the gas consumed start behaving asymptotically (Figure 8(a)). The model captures the inversion of the limiting process from absorption to sealing-up of capillaries (linear to asymptotic trend in Figure 8(a); nearly constant to a dropping trend in Figure 8(d)), whereas the two limitations are actually competitive through a certain range of time $(50 < t < 150\,\text{min})$.

Mass transfer between bulk and particle: influence of particle slip velocity

Mass transfer between bulk and particle limits crystallization if the maximum mass transfer rate is in the same order of magnitude of the experimental gas consumption rate (per particle). In the case of mass transfer being the only limiting process for hydrate formation, then: (i) absorption can be neglected and the bulk concentration tends to the saturation concentration, $C_b \approx H_o f_g$; and

(ii) the resistances of crystal integration can be neglected, thus the concentration at the outer surface of the particle drops to the equilibrium level, $C_{out} \approx H_o f_{eq}$. Using the mass transfer law around spherical particles of Eq. (10):

(C) $-\left.\frac{dn_{g,i}}{dt}\right|_{p/b}^{\max} = 4\pi r_p^2 h_{m,p/b} H_o \left(f_g - f_{eq} \right) >> -\left.\frac{dn_{g,i}}{dt}\right|_{hyd}$, then no particle/bulk mass transfer-limited crystallization

(D) $-\left.\frac{dn_{g,i}}{dt}\right|_{p/b}^{\max} = 4\pi r_p^2 h_{m,p/b} H_o \left(f_g - f_{eq} \right) \approx -\left.\frac{dn_{g,i}}{dt}\right|_{hyd}$, then particle/bulk mass transfer-limited crystallization

Note that: (i) for mass transfer particle/bulk, the gas consumption rate per particle is used $-dn_{g,i}/dt\big|_{hyd}$, instead of the total gas consumption rate of the system $\sum_{i=1}^{n_p}\left(-dn_{g,i}/dt\big|_{hyd}\right)$ as used for understanding limitation of gas absorption in criteria (A,B); (ii) the use of $4\pi r_p^2$ as surface for mass change and $-dn_{g,i}/dt\big|_{hyd} \approx \frac{1}{n_p}\sum_{i=1}^{n_p}\left(-dn_{g,i}/dt\big|_{hyd}\right)$ incur in considering that all particles change mass evenly with the bulk, therefore this criterion does not take particle-particle interactions into consideration.

The key parameter that plays a role on mass transfer limited crystallization is the *relative velocity between the particle and the bulk* (also called *slip velocity*), which is implicit inside the mass transfer coefficient, $h_{m,p/b}\left(\mathrm{Re_p}, \mathrm{Sc}, r_p, D_{g/o}\right)$, with $\mathrm{Re_p}\left(U_{p/b}, r_p, \rho_o, \mu_o\right)$ (see Table 1 for the expression employed). The slip velocity is dependent mainly on the size of the particle, particle/fluid density ratio and continuous phase hydrodynamics[68]. There are some existing correlations for an average solid-liquid flow slip velocity, but here we stick to the use of its limiting

values: (i) the minimum slip is zero, when the fluid carry perfectly the particle (laminar flow, small particles, particle/fluid density ratio near unity); and (ii) the maximum slip is the mixture velocity J, when the mixture cannot carry the particle and it stays stagnant in the pipeline; or yet for a highly turbulent flow (relative motion between eddies).

Figure 9(a) presents sensitivity of the estimated gas consumed over time in means of the slip velocity particle/bulk. It can be observed that even for the no-slip case (red line), mass transfer particle/bulk does not play a role into limiting crystallization. This is again due to the high gas solubility in oil compared to the gas solubility in water (already discussed in Figure 7(c)). Even if the mass transfer coefficient is small and the gas concentration gradient in the mass transfer boundary layer around the particle is high; the gas arrives in a sufficiently high concentration at the oil in the outer surface of the particle; and once it solubilizes in water, there is no considerable change in the furnished gas concentration in water (Figure 9(b), red and black lines).

However, when gas solubility in oil is in the same order of magnitude of gas solubility in water $(H_o \approx H_w)$, then mass transfer particle/bulk may act on limiting crystallization for low mixing systems ($U_{p/b}/J < 1\%$, green and orange lines). This limitation presents a straight line behavior for the gas consumption (Figure 9(a); as observed in literature for water continuous flow[9,12]); and a constant gas consumption rate (Figure 9(d)). The model captures the transition of limitation from mass transfer particle/bulk to the filling-up of capillaries similarly to the discussed in the previous section: (i) when mass transfer particle/bulk limits hydrate formation, then a lower gas concentration in water is furnished to the outer surface of the particles (Figure 9(b)); (ii) the porosity decreases slower in time due to the lower supersaturation furnished to the capillary entrance (Figure 9(c)); (iii) as the porosity attains smaller values, gas is consumed at a lower rate for crystallization and the mass transfer particle/bulk is able to furnish higher supersaturations;

(iv) the limitation process changes from mass transfer particle/bulk to crystallization in the capillaries, characterized by a drop of the total gas consumption rate (Figure 9(d)) and a change in the characteristic trend of the gas consumed over time from linear to asymptotic (Figure 9(a)).

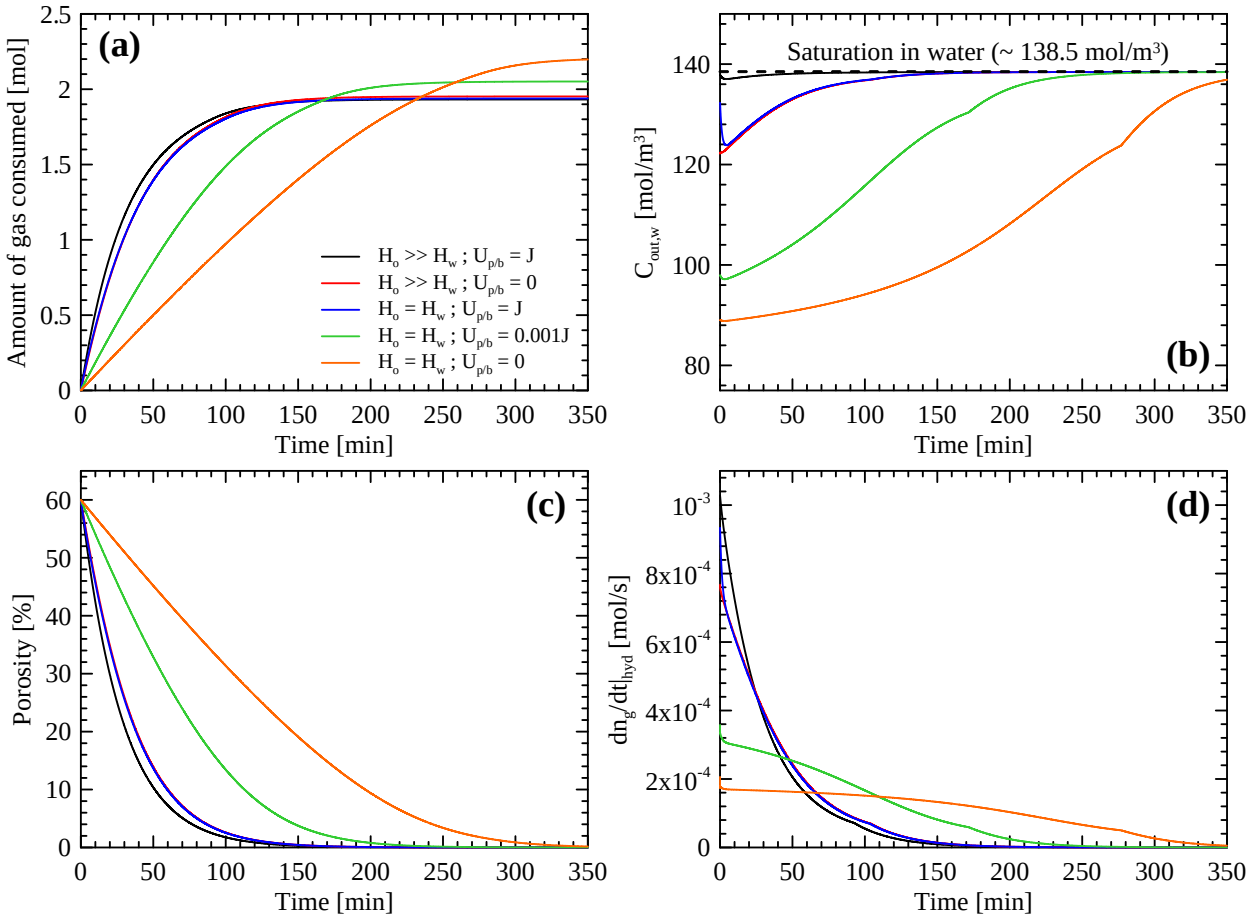

Figure 9: Sensitivity analysis of hydrate formation to slip velocity particle/bulk and for different gas solubility (Henry's constant) in oil and water (H_o, H_w) (other parameters come from Table 1). Evolution in time of: (a) gas consumed due to hydrate formation; (b) gas concentration in the outer surface of the particle inside water; (c) porosity; and (d) gas consumption rate due to hydrate formation. Mass transfer particle/bulk limits crystallization only for low mixing systems and when the gas solubility in the continuous phase is in the same order of gas solubility in water.

At this point, it is possible to conclude that: *(i) given the much higher solubilities of natural gas components (hydrocarbons) in oil than in water; then (ii) the oil continuous phase act as a distributor of gas from the gas-oil interface up to the outer surface of each particle; and (iii) mass transfer particle/bulk and gas/oil absorption processes can be neglected no matter the agitation of the system*. For the case of gas solubility in the continuous phase being in the same order of magnitude of gas solubility in water (e.g., CO_2 hydrates with oil continuous phase; or systems with water continuous phase), then: (i) the influence of absorption and mass transfer particle/bulk can be neglected for highly agitated systems; but (ii) must be considered in lower agitated systems. Notice that gas distribution inside the continuous phase is not accounted in this analysis, which is expected to be higher in dense flows and in systems where the distances between particles and gas-oil interface is large (discussion of α_p -parameter given in section 3; for the results presented, α_p is kept constant, Table 1).

Outer growth vs. crystallization in capillaries: influence of crystal integration constant (k_i)

Whereas absorption and mass transfer particle/bulk act as resistances in series to crystal integration, crystal integration itself is composed of parallel resistances: (i) crystal integration in the capillary walls, which competes with diffusion of gas in water inside the capillary, Eq. (23); and (ii) crystal integration in the outer surface, which can be limited by either water permeation through the hydrate porous media or crystal integration itself due to the supersaturation of gas furnished in the outer surface, Eq. (11). Both (i) and (ii) depends on the porosity of the particle, whereas (i) is determinant on estimating the porosity evolution in time (i.e., the capillary closure time-scale, Eq. (27)).

Here, we want to understand: (i) which crystallization surface is prevailing, outer surface of capillary walls; and (ii) if ever outer growth is prevailing, which is its limiting phenomena (water permeation or crystal integration). By using the second term inside of the minimum function of Eq. (11) to estimate the crystal integration in the outer surface, the following criteria are proposed:

(E) $-dn_{g,i}/dt\big|_{out,cryst\ int} << -dn_{g,i}/dt\big|_{hyd}$, mainly for low values of k_i, then the answer is unique and crystallization in the capillary walls is prevailing. Even if water permeation is high, the maximum gas consumption due to outer growth will be limited by crystal integration. Since this value is much lower than gas consumption due to hydrate formation, then gas consumption in the capillaries is the main phenomena.

(F) $-dn_{g,i}/dt\big|_{out,cryst\ int} > -dn_{g,i}/dt\big|_{hyd}$, mainly for high values of k_i. Two answers exist depending on ζ-value (usually not know a priori): crystallization in the capillary walls (low ζ) or outer growth due to permeation (high ζ). In this case, crystal integration in the outer surface happens too fast to explain hydrate formation, and outer growth must be limited by permeation. There is a maximum value of ζ (non-uniformity of capillary bundle) capable of explaining the experimental results. If ζ is low (capillaries are not well interconnected, thus water permeates slowly to the outer surface), then crystallization in the capillary walls is prevailing over outer growth.

(G) $-\left.\frac{dn_{g,i}}{dt}\right|_{out,cryst\ int} \approx -\left.\frac{dn_{g,i}}{dt}\right|_{hyd}$, mainly for intermediary values of k_i. In this case, three answers are possible: crystallization in the capillary walls, or outer growth limited by either crystal integration or permeation. The answer depends again on ζ. If ζ is high, then crystal integration is the limiting process for outer growth; and since outer growth is in the

same order of magnitude of total gas consumption, than crystallization in the capillary walls is not important. If ζ is low, then outer growth is limited by permeation. If ζ is low enough, then outer growth is almost non-existent and crystallization in capillaries is the main phenomena. For the case of intermediary ζ, all three phenomena may be competitive. It is important to notice, however, that the only phenomena that is mathematically capable of predicting the asymptote in hydrate formation is crystallization in the capillary walls; therefore, if experiments present such asymptote, then this is the limitation step.

The main crystallization surface (outer surface or capillary walls) and the presence or not of water in the outer surface (permeation *vs.* crystal integration) are dependent on k_i and ζ, which are of difficult experimental estimation (and driving-dependent parameters). This explains the difficulty of reproducibility of growth kinetic experiments of gas hydrates commonly reported in literature. The presence of the asymptote on gas consumption of our experiment (Figure 5) points-out crystallization in the capillary walls as limiting phenomenon.

The model and criteria (E,F,G) are used to understand the limiting phenomena for a case of low k_i $(=4.1\times10^{-11}\ \text{mol/(m}^2\text{sPa)}$, as estimated through Eq. (36)) and for a case of high k_i $(=8\times10^{-8}\ \text{mol/(m}^2\text{sPa)}$, as proposed by Al-Otaibi et al.[46,53]). In the case of high k_i, permeation can play a role as the limiting phenomena, and therefore we test sensitivity on ζ-parameter.

Figure 10 and Figure 11 present the gas transfer rates of the different mass transfer resistances for the simulated cases of low and high k_i. The black crosses are the gas consumption rate of the experiment. Independently of k_i, the absorption and mass transfer particle/bulk are negligible (i.e., the maximum gas transfer rates is much higher than the gas consumption rate of the experiment;

as already discussed in the last subsections due to the use of a gas that is much more soluble in oil than in water).

For the low k_i case, the gas consumption in the outer surface (Figure 10(b), blue line) is much lower than the consumption in the capillaries (red line). Therefore, the porosity decrease over time is the main phenomenon in limiting crystallization. This is in agreement with criterion (E). Outer growth is limited by the low crystal integration (characteristic of a low k_i-value), and water always permeate the hydrate porous media and accumulates in the outer surface (Figure 10(c)). *Water accumulation in outer surface is not ideal, since collision between particles then promote capillary bridge formation, making particle to be sticky (wet) and enhancing agglomeration*[3] (see as well discussion in section 5). In the final part of crystallization, when porosity achieves low values, permeation starts to be the limiting process for outer growth (seen as the crossing between red and blue lines of Figure 10(c)). This inversion of limitation process (marked by the gray dashed line) explains the discontinuity of the gas consumption rate in the end of crystallization.

For the high k_i case, Figure 11, and if ever water is always available at the outer surface, then gas hydrate formation due to crystal integration in the outer surface would overpredict the experiments (since $-dn_{g,i}/dt\big|_{out,cryst\ int} > -dn_{g,i}/dt\big|_{hyd}$; Figure 11(a), green > black line). Therefore, water permeation through the porous hydrate particle necessarily limits outer growth (blue and purple lines *vs.* green line). This is in agreement with criterion (F). The water permeation rate is restricted to the use of a ζ-parameter (which is unknown a priori). We plot results for the extreme values of ζ presented in Table 1. In both cases, permeation limits outer growth for the entire crystallization process (blue and purple lines < green line). Yet, growth in capillaries is much more important than outer growth for the considered range of $0.001 \le \zeta \le 0.02$ (red line > blue and

purple lines), and therefore the model presents low sensitivity to ζ (Figure 11(b)). Notice that, since crystal integration is faster for higher k_i, α_p regression converges to lower values $(=8\times10^{-4})$ in order to keep the same initial porosity $(\varepsilon_{in}=60\%)$. Furthermore, the closure time-scale of the capillaries is dependent on k_i (Eq. (27)) and assumes much lower values ($t_{close}\approx 30$ ms for $k_i=8\times10^{-8}$ mol/(m^{2}sPa); $t_{close}\approx 30$ s for $k_i=4.1\times10^{-11}$ mol/(m^{2}sPa)), and therefore the asymptotic behavior of the experiments can only be reached by regressing much lower values of λ-parameter $(1-\lambda=1\times10^{-5})$. Yet, due to outer growth being limited by permeation, all water arriving at the outer surface is instantly crystallized and water would never be available at the outer surface to create capillary bridges. This is a case where agglomeration is reduced. From experiments, however, there exist a certain level of agglomeration, thus the lower values of $k_i \rightarrow 10^{-11}$ mol/(m^{2}sPa) are more likely to explain our experimental results.

As a general conclusion *when considering the range of k_i and ζ of literature, crystallization in capillary walls always prevails over outer growth*. However, *adoption of the different order of magnitude of parameter* $5.5\times10^{-12}\le k_i \le 1.8\times10^{-7}$ mol/(m^{2}sPa) *determines the competition of the limiting phenomena for outer growth between water permeation and crystal integration (which is related to a wet or dry particle, with consequences in agglomeration)*. Low values of k_i incur in outer growth limited by crystal integration, thus water accumulates in the outer surface, turning the particle wet and enhancing agglomeration. High values of k_i incur in outer growth limited by permeation, thus all water arriving in outer surface is instantly crystallized, turning the particle dry and reducing agglomeration.

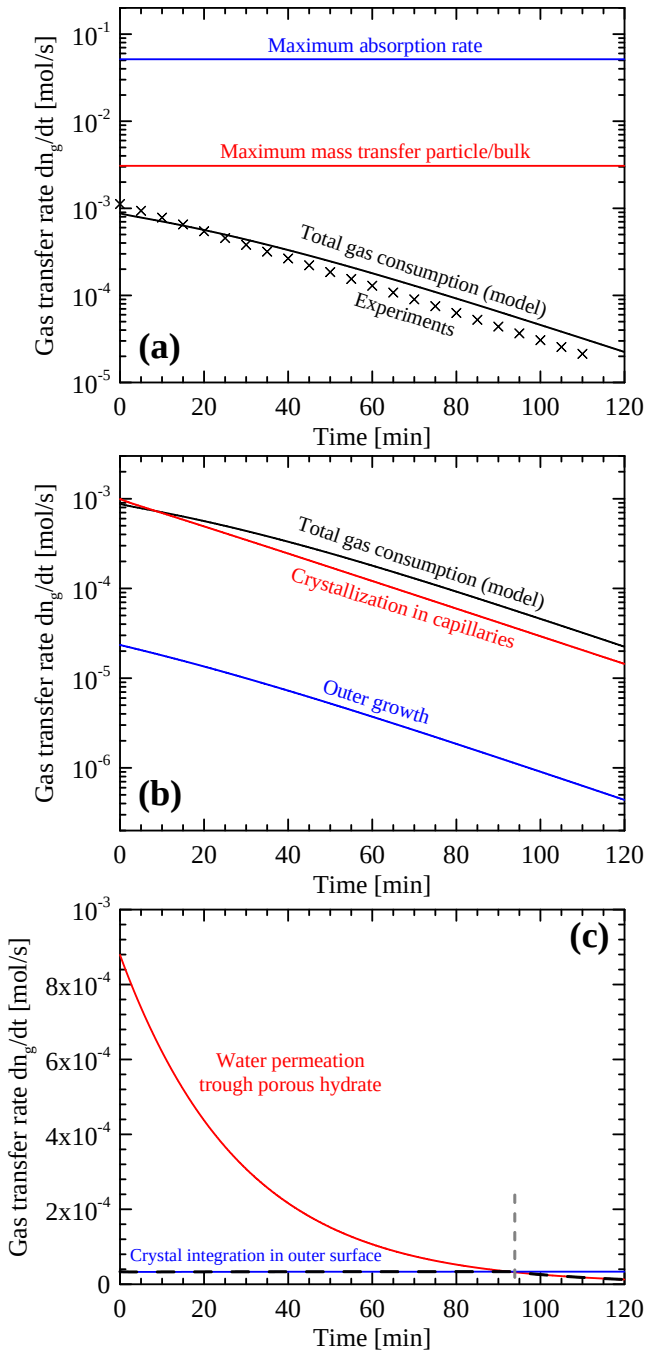

Figure 10: Model evaluation for low crystal integration constant (parameters from Table 1). (a) Absorption and mass transfer particle/bulk *vs.* total gas consumption. (b) Crystallization in capillary walls *vs.* outer growth to predict the total gas consumption. (c) Water permeation *vs.* crystal integration to predict limiting process of outer growth. Crystallization in the capillary walls is the limiting step. Crystal integration limits outer growth for the major part of the process, therefore water accumulates at the outer surface, causing particle to become wet and enhancing agglomeration.

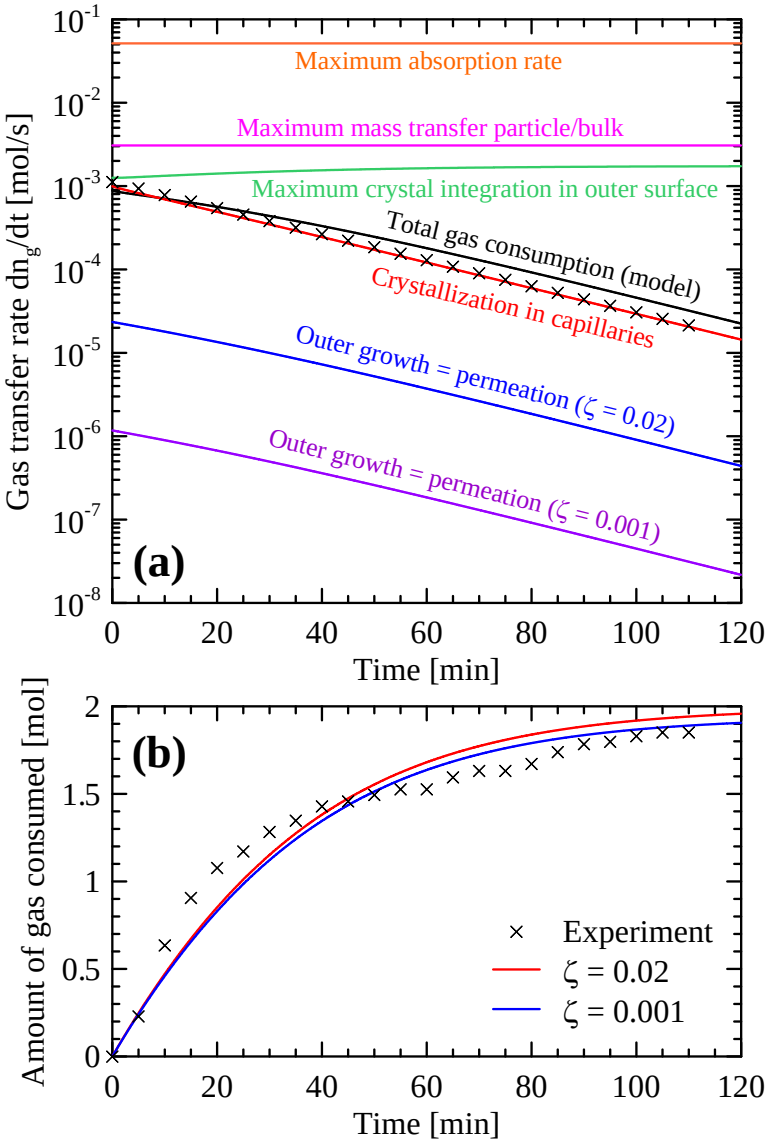

Figure 11: Model evaluation for high crystal integration constant ($k_i = 8\times10^{-8}$ mol/(m^{2}sPa); $\alpha_p = 8\times10^{-4}$; $(1-\lambda = 10^{-5})$; all other parameters from Table 1). (a) Comparison of gas transfer rates of all phenomena against experiments. (b) Amount of gas consumed for extreme values of the range of interconnectivity of capillary bundle $(0.001 \le \zeta \le 0.02)$. Crystallization in the capillary walls is the limiting step, thus (b) is not influenced by ζ. Permeation limits outer growth, thus all water arriving at the outer surface is instantly crystallized, causing particle to become dry and reducing agglomeration.

Influence of driving force, particle size, initial porosity and capillary radius

In this section, we consider the fixed values of Table 1 and test the sensitivity of driving force, particle size (that is, coming from the droplets size determined by the multiphase flow conditions prior to onset of gas hydrates), and the porous media parameters (initial porosity and average capillary radius). Results for the gas consumed over time are shown in Figure 12. The default case (Table 1) is always plotted in black.

Figure 12(a) presents sensitivity to the driving force. The system pressure is kept constant at 80 bar and the temperature is varied from 7 to 1ºC (280.15 to 274.15 K). The methane-water-hydrate equilibrium temperature at this pressure is ~ 10.9ºC (~ 284.05 K), which gives driving force (subcooling) of $3.9 \leq \Delta T \leq 9.9\,\mathrm{K}$. The model captures higher consumption rates for higher driving forces, and the asymptote is reached in less time, explained by a faster sealing of the capillaries. The asymptotic value is the same for all driving forces (~ 2 mol). However, this may not occur in real cases, since higher driving force are related to higher initial porosities and smaller capillary radius (see behaviors of Figure 12(c,d)). The plots in Figure 12(a) do not consider this interaction of driving force *vs.* porous media.

Figure 12(b) presents sensitivity to the particle radius. Smaller particles are related to higher values of the asymptote of gas consumed, but do not interact with its curvature. That is, particle radius act as an inversely proportional linear multiplier of hydrate formation. Particles radius are considered equal to droplet radius prior to nucleation. For a fixed water cut and liquid volume, the number of droplets increase for decreasing droplet size. Since only the outermost part of the particle is actually interacting with crystallization (since gas can penetrate only a limited depth of the capillaries, concept of L_{crit} described in the modeling section), then a higher number of particles means a higher active surface as well. If the droplet size is indefinitely small, then at

some point the absorption process will play a role (otherwise, hydrate would form instantly for very small droplets, which is never observed experimentally even for very high agitated batch reactor systems[13,14]). Estimation of the droplet radius depends on the multiphase flow conditions (mixture velocity, water cut) and fluid properties (viscosity of continuous phase, oil-water interfacial tension). Semi-predictive models for pipeline flow are available in liquid-liquid flow literature[48,69–74] (we suggest Brauner[48] for a comprehensive understanding of the phenomena involved). Yet, agglomeration play a role on particle size and will therefore change the gas consumption rate (not considered in this study).

Figure 12(c) presents the gas consumed over time for different initial porosities of the hydrate particle. Higher initial porosities imply in larger time scales for sealing the particle, affecting the asymptotic value. Therefore, the initial porosity acts as a linear multiplier (directly proportional) of hydrate formation, but do not change its curvature.

Figure 12(d) presents the gas consumed over time for different capillary radius. The initial porosity is kept at a constant value, therefore different capillary sizes imply as well in different number of capillaries per particle (Eq. (31)). The smaller the capillaries, the higher the active surface per unit volume; implying in higher gas consumption rates (inclination of the gas consumed curve). However, smaller capillaries close faster, thus reaching asymptotes in less time (by maintaining the same λ-parameter). Therefore, capillary radius act as a linear multiplier (directly proportional) and curvature changer (inversely proportional) of hydrate formation.

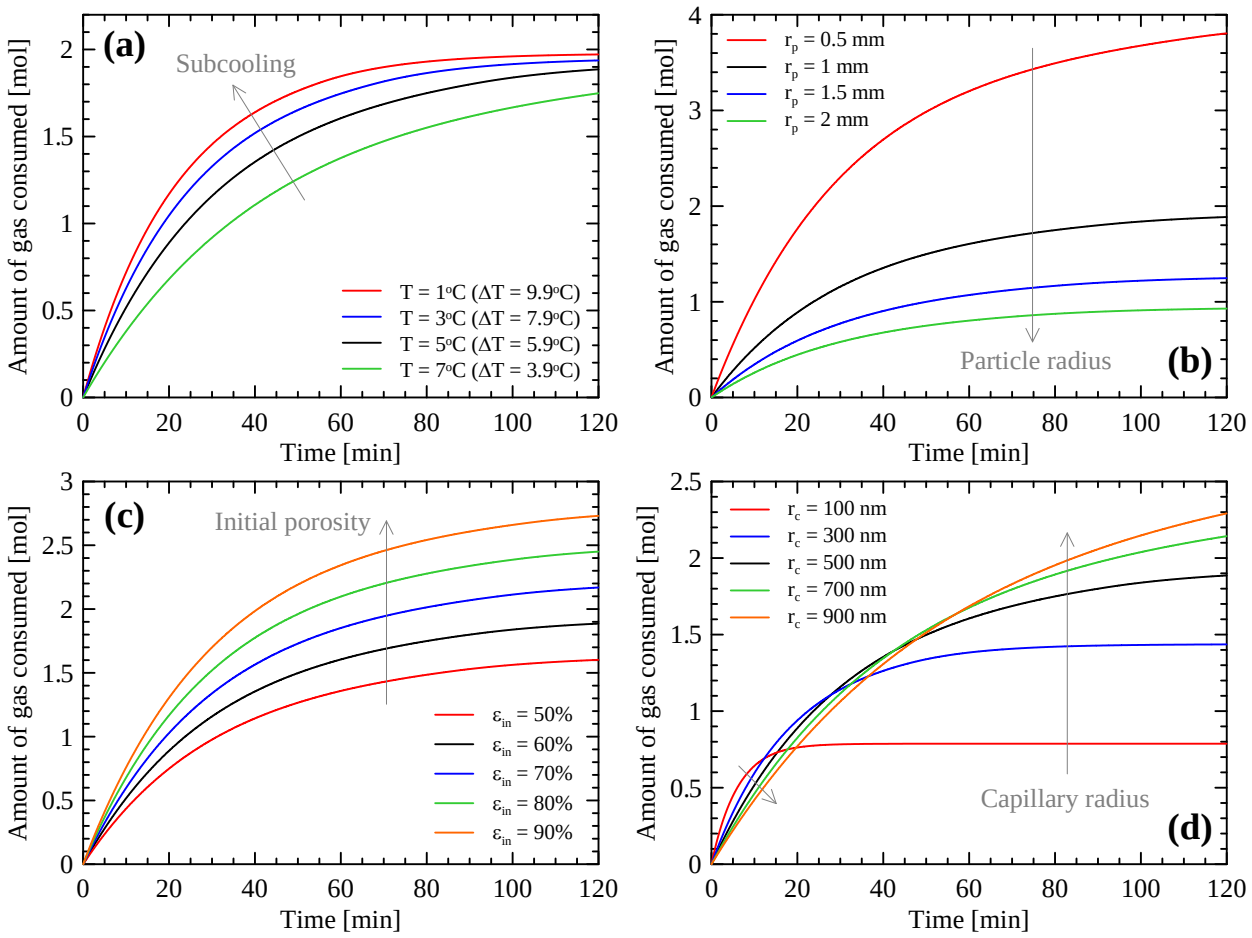

Figure 12: Sensitivity of the model for gas consumed over time based on: (a) driving force/subcooling (different system temperatures, constant pressure of 80×10^5 Pa); (b) particle radius, considered equal to droplet radius prior to hydrate nucleation (agglomeration is neglected); (c) initial porosity of hydrate particle; and (d) capillary radius. All other parameters from Table 1 (black line).

5. Simplified model for CH_4 hydrates in oil continuous flow

Based on the closure values presented in literature for CH_4 hydrates (Table 1), the model can be simplified to the limiting process of hydrate formation, that is, gas consumption in the capillary walls and consequent decrease in porosity with time. The absorption process is not important,

$k_{g/b}A_{g/b}/\forall_b \to \infty$, and the bulk can be considered close to saturation of gas in oil, $C_b \approx H_o f_g$ (that is, $dC_b/dt \to 0$ and there is no need to solve Eq. (4)). The mass transfer between particle and bulk is not important, $h_{m,p/b} \to \infty$, and from Eq. (10) the gas concentration in the outer surface inside oil is close to the bulk one, $C_{out,o} \approx C_b \approx H_o f_g$. Yet, from Eq. (24), $\omega \to 0$. From Eq. (18), solubilization of gas from oil to water in the outer surface of the particles gives $C_{out,w} \approx H_w f_g$, that is, the gas is saturated in water in the outer surface of the particle (concept of oil bulk acting as a distributor of gas from the gaseous free phase up to each particle). Gas consumption in outer surface is negligible compared to the gas consumption due to growth in capillary walls (given the low values for interconnectivity of the porous media, which imply in low permeation rates of water), and therefore Eq. (33) simplifies to $-dn_g/dt\big|_{hyd} \approx \sum_{i=1}^{n_p}\left(-dn_{g,i}/dt\big|_{cap}\right)$. Using Eqs. (23), (31), (32) and (37) in (33):

$$-\left.\frac{dn_g}{dt}\right|_{hyd} = 6\alpha_p \mathrm{WC}\forall_L \frac{\varepsilon_{in}}{r_p}\sqrt{\frac{H_w D_w k_i}{2r_c}}\left(f_g - f_{eq}\right)\exp\left[-(1-\lambda)(\eta+1)\left(f_g - f_{eq}\right)\frac{M_h}{\rho_h}\frac{k_i}{r_c}t\right] \tag{38}$$

For engineering purposes, all the micro-scale unknown parameters related to porous media, crystal integration and gas distribution inside the continuous phase are grouped into two parameters $\varepsilon_{in}, r_c, \lambda, k_i, \alpha_p \to k_1, k_2$:

$$-\left.\frac{dn_g}{dt}\right|_{hyd} = k_1 \frac{\mathrm{WC}\forall_L}{r_p}\sqrt{H_w D_w}\left(f_g - f_{eq}\right)\exp\left[-k_2(\eta+1)\frac{M_h}{\rho_h}\left(f_g - f_{eq}\right)t\right] \tag{39}$$

with:

$$k_1 = 6\alpha_p \varepsilon_{in}\sqrt{\frac{k_i}{2r_c}} = k_1\left(\text{dense or dilute flow, driving force, additives}\right) \tag{40}$$

$$k_2 = (1-\lambda)\frac{k_i}{r_c} = k_2\left(\text{driving force, flow shear, additives}\right) \tag{41}$$

where WC is the water cut; $\forall_L$ is the liquid volume (water + oil); r_p is the particle size (considered equal to droplet size in case of no agglomeration; droplet size comes from Weber and Reynolds number of the continuous phase, which are dependent on mixture flow rate, system water cut and oil-water properties, specially interfacial tension; see correlations proposed by Brauner[48] for engineering applications when droplet size is unknown from experiment); H_w is Henry's constant (solubility form) of the gas inside water (see Sander[17] for compilation of various gases); D_w is the gas diffusivity in water; $\left(f_g - f_{eq}\right)$ is the driving force expressed in fugacity between the gaseous free phase ($f_{g(T,P)}$ is the gas fugacity at system temperature and pressure) and gas-water-hydrate equilibrium ($f_{eq(T,P_{eq})}$ is the gas fugacity at the equilibrium pressure related to system temperature; the relation between equilibrium pressure and system temperature can be retrieved through equilibrium thermodynamics; for engineering purposes, there are commercial software, e.g., Multiflash®[75], PVTsim®[76]); η is the hydration number related to the gas hydrate crystalline structure; $M_h = \left(M_g + \eta M_w\right)/\left(\eta + 1\right)$ is the 'molar mass' of hydrates; ρ_h is the density of a perfect hydrate crystal (no porosity included); and t is time.

As mentioned, the not-easily-found-in-literature parameters are: α_p, which represents the gas distribution inside the continuous phase; ε_{in} the initial porosity of hydrates; k_i the constant of proportionality of the crystallization law (Eq. (1)); r_c the capillary radius; and λ the birth-to-death ratio of capillaries. They are grouped into k_1, k_2, which are independent and assume one unique

value that represents the asymptote (k_1) and the curvature (k_2) of the experimental data of gas consumption over time. By using Table 1, $k_1 = 6.92\times10^{-4}\left[\text{mol/(m}^2\text{sPa)}\right]^{1/2}$ and $k_2 = 1.56\times10^{-6}\,\text{mol/(m}^2\text{sPa)}$ (CH_4 hydrates in light oil continuous flow; this values shall be carefully handled to other scenarios prior to regression with a wider database). Figure 13 (blue line) presents the behavior of Eq. (39) against the experimental results. The model underpredicts the asymptotic value in ~ 11%; that is, all the non-considered phenomena (gas absorption, mass transfer particle/bulk, outer growth) correspond to only 1/10th of the problem.

Since $\varepsilon_{in}, r_c, \lambda, k_i, \alpha_p$ are usually unknown for different gases, then k_1, k_2 shall be regressed directly from the experimental data varying the described parameters of Eqs. (40) and (41), based on the knowledge that: (i) k_i varies with presence of additives (that may block the growing sites and/or associate to the gas/water molecules decreasing their availability to create new crystal growing units); (ii) ε_{in} and r_c are dependent on how fast crystallization occurs, that is, dependent on the driving force and on k_i; (iii) λ is dependent on the squeezing of the particle, related to flow shear, and on how fast crystallization is (driving force, k_i); and (iv) α_p is dependent on the flow being dense or dilute, on the flow shear (flow regime) and on the system size (distance of particles to gas-oil interface). A direct regression of the experimental data gives $k_1 = 7.76\times10^{-4}\left[\text{mol/(m}^2\text{sPa)}\right]^{1/2}$ and the same k_2, and is able to 'correct' the 11% underprediction, red line of Figure 13.

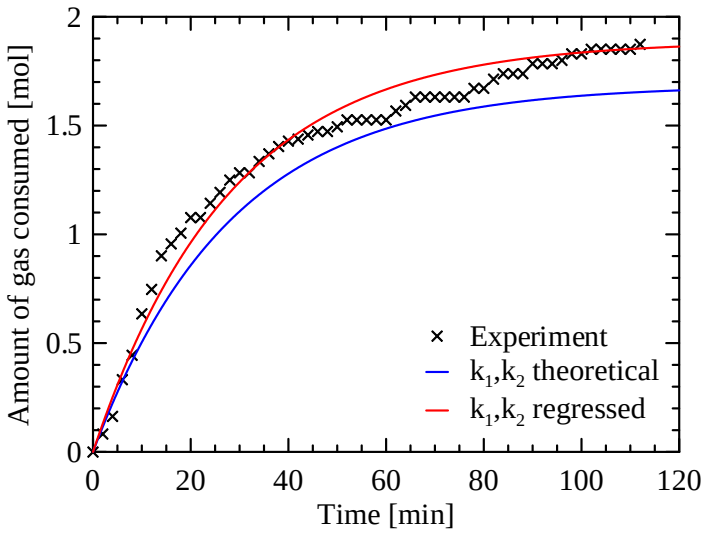

Figure 13: Amount of gas consumed over time predicted by the simplified model, Eq. (39). Blue line: for $k_1 = 6.92\times10^{-4}\left[\text{mol/(m}^2\text{sPa)}\right]^{1/2}$ and $k_2 = 1.56\times10^{-6}\,\text{mol/(m}^2\text{sPa)}$ (theoretical values from Eqs. (40) and (41), closure of Table 1). Red line: $k_1 = 7.76\times10^{-4}\left[\text{mol/(m}^2\text{sPa)}\right]^{1/2}$ and same k_2 (regressed from experimental results using Eq. (39)). The simplified model (crystallization in capillaries as limiting step) describes ~ 90% of the gas hydrate growth kinetics (CH_4 in oil continuous flow).

The shape of Eq. (39) is similar to the Arrhenius-type expression commonly employed in gas hydrate literature, $-\left.\frac{dn_g}{dt}\right|_{hyd} \propto \Delta f \exp\left(\Delta f^{-1}\right) \approx \Delta T \exp\left(\Delta T^{-1}\right)$ [22,77–82], where driving force in both expressions appears as a linear multiplier plus an inversely proportional multiplier inside an exponential function. The approach herein used further highlights the influence of: (i) multiphase flow (water cut and droplet size prior to nucleation); (ii) gas solubility and gas diffusion in water (that is, gas guest properties used to form hydrates); (iii) hydrate structure (related to different

hydration numbers); and (iv) porosity decrease in time, causing an exponential time-dependent term.

Yet, the model can be used to understand agglomeration. *In order to reduce agglomeration, liquid bridge formation between particles shall be avoided. This occurs when permeation limits outer growth, therefore all water arriving at the outer surface of the particle instantly crystallizes*. Using the competitive phenomena inside the minimum function of Eq. (9) and neglecting the absorption and particle/bulk mass transfer resistances (so the driving force is $(f_g - f_{eq})$):

$$\mathrm{Da}_{\mathrm{hyd}} = \frac{\text{crystallization}}{\text{permeation}} = \frac{A_i k_i \left(f_g - f_{eq} \right)}{\dfrac{\rho_w}{\eta M_w} Q} > 1 \text{ avoids agglomeration} \tag{42}$$

where Q is the water permeation flowrate in one particle, expressed by Eq. (5), and A_i is the outer surface of the particle ($4\pi r_p^2$ for spherical particles). Equation (42) is a modified Damköhler number applied to agglomeration of gas hydrates, and expresses the competition between crystallization integration in the outer surface of the particle and permeation of water through the hydrate porous media. This expression can be expanded to (coming from Eq. (11) instead of Eq. (9)):

$$\frac{1}{12} \underbrace{\left(\frac{\rho_w}{\mu_w M_w} \right)}_{\text{water prop.}} \underbrace{\left(\frac{\zeta \varepsilon r_c}{\tau^2} \right)}_{\text{hyd. porous media}} \underbrace{r_p^{-1} k_i^{-1}}_{\text{flow cryst.}} \underbrace{\left(f_g - f_{eq} \right)^{-1}}_{\text{subcooling}} \underbrace{\eta^{-1}}_{\text{hyd. struct.}} \underbrace{\left(\sigma_{o/w} \cos \theta_{o/w/h} \right)}_{\text{interfacial prop.}} < 1 \text{ avoids agglomeration} \tag{43}$$

valid for hydrophilic hydrates ($\theta_{o/w/h} < 90^o$; if the use of surfactant additives is able to change wettability, then water permeation is completely avoided, as discussed in the first part of this series[3]). Criterion (43) evidences that agglomeration is reduced when: (i) driving forces are higher and crystal integration is faster (concept of cold flow[83]); (ii) oil-water interfacial tensions are

smaller and wetted angles oil-water-hydrate are higher (effect of surfactant additives[3]); and (iii) capillary radius is smaller and capillary tortuosity is higher (associated to the driving force).

6. Conclusions

This article gives mathematical description of the mass transfer system of gas hydrate growth kinetics. Closure of the model depends on five (05) unknown micro-scale parameters $\varepsilon_{in}, r_c, \lambda, k_i, \alpha_p$, but the range of closure values reported in literature for CH_4 hydrates in oil continuous flow points out crystallization in the capillary walls (with related porosity decrease) to be the limiting step of crystallization. Simplification of the model reduces closure to two (02) independent parameters (k_1, k_2) that come from experimental regression. The simplified model captures ~ 90% of the gas consumption trend observed in a case-test of hydrate formation in a flowloop. It is expected that this simplified-shaped equation is consistent with different gases in oil continuous flow as long as the gas solubility in oil is much larger than in water $(H_o >> H_w$; i.e., application for other hydrocarbon gases, but further regression of k_1, k_2 is needed).

The main conclusions about the mass transfer phenomena related to growth kinetics are:

- Inner growth (if ever a shelled particle exists) happens only when $\mathrm{Ha_c} L_c / r_c < 2.5$, which is highly improbable given the range of closure parameters furnished in literature.
- The capillaries, the outer surface of the particles and the mixture bulk can be considered at thermal equilibrium and thus heat transfer limitation is only due to mixture heat exchange with pipeline wall and outer medium/ocean (conclusion from Supporting Material).
- When gas solubility in the continuous phase is much higher than gas solubility in water ($H_o \gg H_w$; e.g., hydrocarbon gases; counter-examples are gases with high affinity in water,

like CO_2, or when the continuous phase is water), then absorption and mass transfer particle/bulk can be neglected.

- Sealing-up of capillaries (porosity decrease with time) is the only phenomenon that is mathematically capable of explaining the asymptotic trend of gas consumed over time.
- Comprehension of the limiting step of outer growth (permeation *vs.* crystal integration) is key to understand if particle is wet or dry, with consequences on agglomeration and plugging.

Corresponding authors

*Amadeu K. Sum, asum@mines.edu

*Rigoberto E.M. Morales, rmorales@utfpr.edu.br

*Ana Cameirão, cameirao@emse.fr

Acknowledgements

The research groups are part of the Joint International Research Program on Gas Hydrates and Multiphase Flow. The authors acknowledge the financial support of Région AURA Auvergne Rhône-Alpes through the project COOPERA FluEnergy, the Institut Mines-Télécom, the Coordination for the Improvement of Higher Education Personnel - Brazil (CAPES) - Finance Code 001, and TE/CENPES/PETROBRAS (5850.0103370.17.9). CLB thanks the support of M.Sc. Vinícius Rodrigues de Almeida and M.Sc. Rafael Fabrício Alves in measuring and video recording gas hydrate formation in the flow loop at MSE.

Nomenclature

Roman letters

A	Surface area	[m^2]
$A_{g/b}$	Interfacial surface between gas and bulk	[m^2]
B_c	Birth rate of capillaries	[s^{-1}]
$\bar{C}$	Dimensionless driving force, also called supersaturation, Eq. (16)	[-]
C_b	Gas concentration in the bulk	[mol/m^3]
$C_{g/o}$	Gas concentration at the gas-bulk interface	[mol/m^3]
$C_{out,w}, C_{out,o}$	Gas concentration at the outer surface of the particle inside water/oil	[mol/m^3]
Da_{hyd}	Modified Damköhler number for agglomeration of gas hydrates, which expresses competition between crystallization in the outer surface of particle and water permeation through porous particle	[-]
D_c	Death rate of capillaries	[s^{-1}]
D_w, D_o	Gas diffusivity in water/oil	[m^2/s]
f_g	Gas fugacity in gaseous free phase evaluated at system pressure and temperature, $f_g(P,T)$	[Pa]
f_{eq}	Gas fugacity at gas-water-hydrate equilibrium, evaluated at system temperature and its related equilibrium pressure, $f_{eq}(P_{eq},T)$	[Pa]

Ha_c	Hatta number of capillaries, dimensionless number that represents competition between crystallization in capillary walls and diffusion of gas through water trapped in the capillaries, Eq. (14)	[-]
H_w, H_o	Henry's constant of gas inside phase water/oil, given in the solubility form $H = C/f$	[mol/(m^{3}Pa)]
$h_{p/b}$	Heat transfer coefficient between particle and bulk	[W/(m^{2}K)]
$h_{m,p/b}$	Mass transfer coefficient between particle and bulk	[m/s]
Δh_{hyd}	Enthalpy of formation of gas hydrates	[J/mol of gas]
J	Mixture velocity	[m/s]
k_w, k_o	Thermal conductivity of water/oil	[W/(m.K)]
K	Permeability of porous media	[m^2]
k_i	Constant of proportionality of crystal integration (intrinsic kinetics), given by the crystallization law of Eq. (1)	[mol/(m^{2}sPa)]
k_{abs}	Absorption coefficient of gas by the bulk	[m/s]
L_c	Capillary length	[m]
$\bar{L}_c$	Capillary dimensionless length, $\bar{L}_c = L_c / r_c$	[m]
L_{crit}	Gas penetration length inside capillaries, critical length over which shell width would never cause core shrinkage, $L_{crit} = 2.5 r_c / Ha_c$	[m]
M	Molar mass	[kg/mol]
n_c	Number of capillaries per particle	[-]
n_d	Number of droplets prior to onset of hydrate formation	[-]

n_p	Number of particles in the system	[-]
$-dn_g/dt\|_{abs}$	Gas transfer rate due to gas absorption by the bulk (for the entire system)	[mol/s]
$-dn_{g,i}/dt\|_{1cap}$	Gas consumption rate in one capillary of one particle *i*	[mol/s]
$-dn_g/dt\|_{cap}$	Gas consumption rate in due to crystallization in the capillary walls (all particles)	[mol/s]
$-dn_g/dt\|_{hyd}$	Total gas consumption rate due to hydrate formation (all particles)	[mol/s]
$-dn_{g,i}/dt\|_{hyd}$	Gas consumption rate due to hydrate formation in one particle *i*	[mol/s]
$-dn_{g,i}/dt\|_{p/b}$	Gas transfer rate due to mass transfer bulk/particle in one particle *i*	[mol/s]
$-dn_{g,i}/dt\|_{out}$	Gas consumption rate in outer surface of one particle *i* (cryst int: due to crystal integration in outer growth; perm: due to permeation of water through porous hydrate)	[mol/s]
dn_h/dt	Hydrate formation rate	[mol/s]
$-dn_w/dt\|_{hyd}$	Water consumption rate due to hydrate formation	[mol/s]
N''	Gas flux	[mol/(m^{2}s)]
P	Pressure	[Pa]
Pr	Prandtl number	[-]
$-\Delta P_c$	Capillary induced pressure	[Pa]
Q	Water permeation flow rate through the porous hydrate	[m^3/s]
$\dot{Q}_{hyd}$	Heat release due to hydrate formation (all particles)	[W]

$\dot{Q}_{hyd,i}$	Heat release due to hydrate formation in one particle	[W]
$\dot{Q}_{hyd,1cap}$	Heat release due to hydrate formation in one capillary of one particle	[W]
Re	Reynolds number	[-]
Sc	Schmidt number	[-]
Sh	Sherwood number	[-]
r_c	Capillary radius	[m]
$\overline{r}_c$	Dimensionless capillary radius	[m]
r_d	Droplet radius	[m]
r_{in} , r_{out}	Inner and outer radius in the case of a shelled hydrate particle	[m]
r_p	Particle radius	[m]
dr_p/dt	Linear outer growth velocity of the particle	[m/s]
t	Time	[s]
t_{close}	Time-scale for capillary closure, Eq. (27)	[s]
T	Temperature	[K]
T_b	Temperature of bulk	[K]
T_c	Temperature of capillary wall	[K]
T_{out}	Temperature of outer surface of particle	[K]
$U_{p/b}$	Relative/slip velocity between particle and bulk	[m/s]
$\forall_b$, $\forall_L$	Volume of bulk (oil), volume of liquid (oil + water)	[m^3]
WC	Water cut, ratio of water to (water + oil) flow rates, $\mathrm{WC} = Q_w/(Q_w + Q_o)$	[-]

z	Axial direction of the capillary, pointing inwardly to the particle	[m]
$\overline{z}$	Dimensionless axial direction of the capillary, Eq. (15)	[-]
$\overline{z}_c$	Dimensionless capillary length, $\overline{z}_c = L_c / r_c$	[-]

Greek letters

α_p	Efficiency of particles interacting with the bulk, Eq. (37)	[-]
ε	Hydrate porosity (ε_{in} is initial porosity)	[-]
η	Hydration number, given by the 'stoichiometric' relation $1G + \eta H_2O \rightarrow (1+\eta)\, Hyd$ [mol of H_2O / mol of hyd]	
λ	Capillary birth-to-death ratio, Eq. (29)	[-]
μ	Dynamic viscosity	[Pa.s]
$\theta_{o/w/h}$	Oil-water-hydrate wetted angle (water side), $\theta_{o/w/h} < 90^o$ (hydrophilic hydrates)	[-]
ρ	Density	[kg/m^3]
$\sigma_{o/w}$	Oil-water interfacial tension	[J/m^2]
τ	Capillary tortuosity	[-]
ω	Dimensionless parameter that represents competition between mass transfer particle/bulk and crystallization in the capillaries, Eq. (24)	[-]
ζ	Interconnectivity of capillaries, non-uniformities due to capillary bundle geometry, Eq. (6)	[-]

Indexes

abs Absorption

b Bulk

c Capillary

d Droplet

cap Crystallization in capillary walls

eq Three-phase gas-water-hydrate equilibrium

g Gas

h Gas hydrates

hyd Hydrate formation

i Referent to one particle

o Oil

p Hydrate particle

sat Gas saturation (o: in oil; w: in water)

w Water

Supporting information

A supporting information file is available, which proves the hypothesis of thermal equilibrium between capillaries, particles and bulk, and presents some mathematical demonstrations of the model.

References

(1) Sum, A. K.; Koh, C. A.; Sloan, E. D. Clathrate Hydrates: From Laboratory Science to Engineering Practice. *Ind. Eng. Chem. Res.* **2009**, *48* (16), 7457–7465. https://doi.org/10.1021/ie900679m.

(2) Cardoso, C. A. B. R.; Gonçalves, M. A. L.; Camargo, R. M. T. Design Options for Avoiding Hydrates in Deep Offshore Production. *J. Chem. Eng. Data* **2015**, *60*, 330–335. https://doi.org/10.1021/je500601f.

(3) Bassani, C. L.; Melchuna, A. M.; Cameirão, A.; Herri, J.-M.; Morales, R. E. M.; Sum, A. K. A Multiscale Approach for Gas Hydrates Considering Structure, Agglomeration, and Transportability under Multiphase Flow Conditions: I. Phenomenological Model. *Ind. Eng. Chem. Res.* **2019**, *58* (31), 14446–14461. https://doi.org/10.1021/acs.iecr.9b01841.

(4) Li, S.-L.; Wang, Y.-F.; Sun, C.-Y.; Chen, G.-J.; Liu, B.; Li, Z.-Y.; Ma, Q.-L. Factors Controlling Hydrate Film Growth at Water/Oil Interfaces. *Chem. Eng. Sci.* **2015**, *135*, 412–420. https://doi.org/10.1016/J.CES.2015.01.057.

(5) Melchuna, A.; Cameirao, A.; Herri, J. M.; Glenat, P. Topological Modeling of Methane Hydrate Crystallization from Low to High Water Cut Emulsion Systems. *Fluid Phase Equilib.* **2016**, *413*, 158–169. https://doi.org/10.1016/j.fluid.2015.11.023.

(6) Ding, L.; Shi, B.; Lv, X.; Liu, Y.; Wu, H.; Wang, W.; Gong, J. Investigation of Natural Gas Hydrate Slurry Flow Properties and Flow Patterns Using a High Pressure Flow Loop. *Chem. Eng. Sci.* **2016**, *146*, 199–206. https://doi.org/10.1016/j.ces.2016.02.040.

(7) Ding, L.; Shi, B.; Lv, X.; Liu, Y.; Wu, H.; Wang, W.; Gong, J. Hydrate Formation and Plugging Mechanisms in Different Gas-Liquid Flow Patterns. *Ind. Eng. Chem. Res.* **2017**, *56* (14), 4173–4184. https://doi.org/10.1021/acs.iecr.6b02717.

(8) Chen, J.; Yan, K.-L.; Chen, G.-J.; Sun, C.-Y.; Liu, B.; Ren, N.; Shen, D.-J.; Niu, M.; Lv,

Y.-N.; Li, N.; et al. Insights into the Formation Mechanism of Hydrate Plugging in Pipelines. *Chem. Eng. Sci.* **2015**, *122*, 284–290. https://doi.org/10.1016/j.ces.2014.09.039.

(9) Englezos, P.; Kalogerakis, N.; Dholabhai, P. D.; Bishnoi, P. R. R. Kinetics of Formation of Methane and Ethane Gas Hydrates. *Chem. Eng. Sci.* **1987**, *42* (11), 2647–2658. https://doi.org/10.1016/0009-2509(87)87015-X.

(10) Englezos, P.; Kalogerakis, N.; Dholabhai, P. D.; Bishnoi, P. R. Kinetics of Gas Hydrate Formation from Mixtures of Methane and Ethane. *Chem. Eng. Sci.* **1987**, *42* (11), 2659–2666. https://doi.org/10.1016/0009-2509(87)87016-1.

(11) Skovborg, P.; Rasmussen, P. A Mass Transport Limited Model for the Growth of Methane and Ethane Gas Hydrates. *Chem. Eng. Sci.* **1994**, *49* (8), 1131–1143. https://doi.org/10.1016/0009-2509(94)85085-2.

(12) Herri, J. M.; Pic, J. S.; Gruy, F.; Cournil, M. Methane Hydrate Crystallization Mechanism from In-Situ Particle Sizing. *AIChE J.* **1999**, *45* (3), 590–602. https://doi.org/10.1002/aic.690450316.

(13) Turner, D. J.; Miller, K. T.; Dendy Sloan, E. Methane Hydrate Formation and an Inward Growing Shell Model in Water-in-Oil Dispersions. *Chem. Eng. Sci.* **2009**, *64* (18), 3996–4004. https://doi.org/10.1016/j.ces.2009.05.051.

(14) Shi, B. H.; Gong, J.; Sun, C. Y.; Zhao, J. K.; Ding, Y.; Chen, G. J. An Inward and Outward Natural Gas Hydrates Growth Shell Model Considering Intrinsic Kinetics, Mass and Heat Transfer. *Chem. Eng. J.* **2011**, *171* (3), 1308–1316. https://doi.org/10.1016/j.cej.2011.05.029.

(15) Shindo, Y.; Sakaki, K.; Fujioka, Y.; Komiyama, H. Kinetics of the Formation of CO2 Hydrate on the Surface of Liquid CO2 Droplet in Water. *Energy Convers. Manag.* **1996**,

37 (4), 485–489. https://doi.org/10.1016/0196-8904(95)00198-0.

(16) Kashchiev, D.; Firoozabadi, A. Driving Force for Crystallization of Gas Hydrates. *J. Cryst. Growth* **2002**, *241* (1–2), 220–230. https://doi.org/10.1016/S0022-0248(02)01134-X.

(17) Sander, R. Compilation of Henry's Law Constants (Version 4.0) for Water as Solvent. *Atmos. Chem. Phys.* **2015**, *15*, 4399–4981. https://doi.org/10.5194/acp-15-4399-2015.

(18) Smith, F. L.; Harvey, A. H. Avoid Common Pitfalls When Using Henry's Law. *Chem. Eng. Process* **2007**, *103* (9), 33–39.

(19) Mersmann, A. *Crystallization Technology Handbook - Second Edition Revised and Expanded*, 2nd ed.; Marcel Dekker Inc.: New York, 2001.

(20) Kashchiev, D.; Firoozabadi, A. Nucleation of Gas Hydrates. *J. Cryst. Growth* **2002**, *243* (3–4), 476–489. https://doi.org/10.1016/S0022-0248(02)01576-2.

(21) Sampaio, T. P.; Tavares, F. W.; Lage, P. L. C. Non-Isothermal Population Balance Model of the Formation and Dissociation of Gas Hydrates. *Chem. Eng. Sci.* **2017**, *163*, 234–254. https://doi.org/10.1016/j.ces.2016.12.012.

(22) Bassani, C. L.; Barbuto, F. A. A.; Sum, A. K.; Morales, R. E. M. A Three-Phase Solid-Liquid-Gas Slug Flow Mechanistic Model Coupling Hydrate Dispersion Formation with Heat and Mass Transfer. *Chem. Eng. Sci.* **2018**, *178*, 222–237. https://doi.org/10.1016/j.ces.2017.12.034.

(23) Ramkrishna, D. *Population Balances: Theory and Applications to Particulate Systems in Engineering*, 1st ed.; San Diego, 2000.

(24) Balakin, B. V.; Hoffmann, A. C.; Kosinski, P. Population Balance Model for Nucleation, Growth, Aggregation, and Breakage of Hydrate Particles in Turbulent Flow. *AIChE J.*

2010, *56* (8), 2052–2062. https://doi.org/10.1002/aic.12122.

(25) Balakin, B. V.; Lo, S.; Kosinski, P.; Hoffmann, A. C. Modelling Agglomeration and Deposition of Gas Hydrates in Industrial Pipelines with Combined CFD-PBM Technique. *Chem. Eng. Sci.* **2016**, *153*, 45–57. https://doi.org/10.1016/j.ces.2016.07.010.

(26) Straume, E. O. Study of Gas Hydrate Formation and Wall Deposition under Multiphase Flow Conditions, PhD Thesis, Federal University of Technology - Paraná, Curitiba, Brazil, 2017.

(27) Mori, Y. H.; Mochizuki, T. Mass Transport across Clathrate Hydrate Films - a Capillary Permeation Model. *Chem. Eng. Sci.* **1997**, *52* (20), 3613–3616. https://doi.org/10.1016/S0009-2509(97)00169-3.

(28) Hirata, A.; Mori, Y. H. How Liquids Wet Clathrate Hydrates: Some Macroscopic Observations. *Chem. Eng. Sci.* **1998**, *53* (14), 2641–2643. https://doi.org/10.1016/S0009-2509(98)00078-5.

(29) Dullien, F. A. L. *Porous Media: Fluid Transport and Pore Structure*, 1st ed.; Press, A., Ed.; Academic Press: New York, 1979.

(30) Civan, F. *Porous Media Transport Phenomena*, 1st ed.; Wiley, Ed.; Wiley: Hoboken, New Jersey, 2011.

(31) Kozeny, J. Über Kapillare Leitung Des Wassers Im Boden. *Akad. des Wissenschaften Wien* **1927**, *136* (2a), 271–306.

(32) Carman, P. C. Fluid Flow through Granular Beds. *Trans. Inst. Chem. Eng.* **1937**, *15*, S32–S48. https://doi.org/10.1016/S0263-8762(97)80003-2.

(33) Espitalier, F.; David, R.; Schwartzentruber, J.; Baillon, F.; Gaunand, A.; Cournil, M.; Gruy, F.; Cameirão, A. Les Fondamentaux de la Cristallisation et de la Précipitation

nte.mines-albi.fr/CristalGemme/co/CristalGemme.html (accessed Jan 25, 2018).

(34) David, R.; Espitalier, F.; Cameirão, A.; Rouleau, L. Developments in the Understanding and Modeling of the Agglomeration of Suspended Crystals in Crystallization from Solutions. *KONA Powder Part. J.* **2003**, *21*, 40–53. https://doi.org/10.14356/kona.2003008.

(35) Shindo, Y.; Lund, P. C.; Fujioka, Y.; Komiyama, H. Kinetics and Mechanism of the Formation of CO2 Hydrate. *Int. J. Chem. Kinet.* **1993**, *25* (9), 777–782. https://doi.org/10.1002/kin.550250908.

(36) Lund, P. C.; Shindo, Y.; Fujioka, Y.; Komiyama, H. Study of the Pseudo-Steady-State Kinetics of CO2 Hydrate Formation and Stability. *Int. J. Chem. Kinet.* **1994**, *26* (2), 289–297. https://doi.org/10.1002/kin.550260207.

(37) Shindo, Y.; Lund, P. C.; Fujioka, Y.; Komiyama, H. Kinetics of Formation of CO2 Hydrate. *Energy Convers. Manag.* **1993**, *34* (9–11), 1073–1079. https://doi.org/10.1016/0196-8904(93)90055-F.

(38) Teng, H.; Kinoshita, C. M.; Masutani, S. M. Hydrate Formation on the Surface of a CO2 Droplet in High-Pressure, Low-Temperature Water. *Chem. Eng. Sci.* **1995**, *50* (4), 559–564. https://doi.org/10.1016/0009-2509(94)00438-W.

(39) Bird, R. B.; Stewart, W. E.; Lightfoot, E. N. *Transport Phenomena*, 2nd ed.; John Wiley & Sons, 2002.

(40) Bassani, C. L.; Cameirão, A.; Herri, J.-M.; Sum, A. K.; Morales, R. E. M. Revisited Model for Inward and Outward Growth of Gas Hydrate Particles in Water-in-Oil Emulsions. In *17th Brazilian Congress of Thermal Sciences and Engineering*; ABCM: Águas de Lindóia, Brazil, 2018; p ENCIT-2018-0491.

(41) Lv, Y.-N.; Sun, C.-Y.; Liu, B.; Chen, G.-J.; Gong, J. A Water Droplet Size Distribution Dependent Modeling of Hydrate Formation in Water/Oil Emulsion. *AIChE J.* **2017**, *63* (3), 1010–1023. https://doi.org/10.1002/aic.15436.

(42) Melchuna, A. M. Experimental Study and Modeling of Methane Hydrates Crystallization under Flow from Emulsions with Variable Fraction of Water and Anti-Agglomerant, PhD Thesis, Mines Saint-Etienne, Saint-Etienne, France, 2016.

(43) Joshi, S. V.; Grasso, G. A.; Lafond, P. G.; Rao, I.; Webb, E.; Zerpa, L. E.; Sloan, E. D.; Koh, C. A.; Sum, A. K. Experimental Flowloop Investigations of Gas Hydrate Formation in High Water Cut Systems. *Chem. Eng. Sci.* **2013**, *97*, 198–209. https://doi.org/10.1016/j.ces.2013.04.019.

(44) Total. *Kerdane D 75: Safety Data Sheet*; 2015.

(45) Bergeron, S.; Beltrán, J. G.; Servio, P. Reaction Rate Constant of Methane Clathrate Formation. *Fuel* **2010**, *89* (2), 294–301. https://doi.org/10.1016/j.fuel.2009.06.019.

(46) Al-Otaibi, F. D. Kinetic Studies of Gas Hydrate Formation Using in Situ Particles Size Analysis and Raman Spectroscopy, PhD Thesis, University of Calgary, Calgary, Canada, 2009.

(47) Sharma, S. Gas Hydrate Particle Size Measurements, MSc Thesis, University of Calgary, Calgary, Canada, 1996.

(48) Brauner, N. The Prediction of Dispersed Flows Boundaries in Liquid-Liquid and Gas-Liquid Systems. *Int. J. Multiph. Flow* **2001**, *27* (5), 885–910. https://doi.org/10.1016/S0301-9322(00)00056-2.

(49) Kashchiev, D.; Firoozabadi, A. Induction Time in Crystallization of Gas Hydrates. *J. Cryst. Growth* **2003**, *250* (3–4), 499–515. https://doi.org/10.1016/S0022-0248(02)02461-

2.

(50) Ding, L.; Shi, B.; Wang, J.; Liu, Y.; Lv, X.; Wu, H.; Wang, W.; Lou, X.; Gong, J. Hydrate Deposition on Cold Pipe Walls in Water-in-Oil (W/O) Emulsion Systems. *Energy & Fuels* **2017**, *31* (9), 8865–8876. https://doi.org/10.1021/acs.energyfuels.7b00559.

(51) Klapp, S. A.; Hemes, S.; Klein, H.; Bohrmann, G.; MacDonald, I.; Kuhs, W. F. Grain Size Measurements of Natural Gas Hydrates. *Mar. Geol.* **2010**, *274* (1–4), 85–94. https://doi.org/10.1016/J.MARGEO.2010.03.007.

(52) Staykova, D. K.; Kuhs, W. F.; Salamatin, A. N.; Hansen, T. Formation of Porous Gas Hydrates from Ice Powders: Diffraction Experiments and Multistage Model. *J. Phys. Chem. B* **2003**, *107* (37), 10299–10311. https://doi.org/10.1021/jp027787v.

(53) Al-Otaibi, F.; Clarke, M.; Maini, B.; Bishnoi, P. R. Kinetics of Structure II Gas Hydrate Formation for Propane and Ethane Using an In-Situ Particle Size Analyzer and a Raman Spectrometer. *Chem. Eng. Sci.* **2011**, *66*, 2468–2474. https://doi.org/10.1016/j.ces.2011.03.012.

(54) Srivastan, S.; Darwish, N. A.; Gasem, K. A. M.; Robinson Jr., R. L. Solubility of Methane in Hexane, Decane, and Dodecane at Temperatures from 311 to 423 K and Pressures to 10.4 MPa. *J. Chem. Eng. Data* **1992**, *37* (4), 516–520. https://doi.org/10.1021/je00008a033.

(55) Jung, J. W.; Espinoza, D. N.; Santamarina, J. C. Properties and Phenomena Relevant to CH4-CO2 Replacement in Hydrate-Bearing Sediments. *J. Geophys. Res. Solid Earth* **2010**, *115*, B10102. https://doi.org/10.1029/2009JB000812.

(56) Sloan, E. D.; Koh, C. A. *Clathrate Hydrates of Natural Gases*, 3rd ed.; Taylor & Francis Group: Boca Raton, United States, 2008.

(57) Lemmon, E. W.; Huber, M. L.; McLinden, M. O. REFPROP Reference Fluid Thermodynamic and Transport Properties. NIST Standard Reference Database 23 2013.

(58) Setzmann, U.; Wagner, W. A New Equation of State and Tables of Thermodynamic Properties for Methane Covering the Range from the Melting Line to 625 K at Pressures up to 1000 MPa. *J. Phys. Chem. Ref. Data* **1991**, *20* (6), 1061–1155. https://doi.org/10.1063/1.555898.

(59) Engineering Toolbox. Diffusion coefficients of gases in water https://www.engineeringtoolbox.com/diffusion-coefficients-d_1404.html (accessed Jan 17, 2019).

(60) Straume, E. O.; Kakitani, C.; Merino-Garcia, D.; Morales, R. E. M.; Sum, A. K. Experimental Study of the Formation and Deposition of Gas Hydrates in Non-Emulsifying Oil and Condensate Systems. *Chem. Eng. Sci.* **2016**, *155*, 111–126. https://doi.org/10.1016/j.ces.2016.07.046.

(61) Ghanbarian, B.; Hunt, A. G.; Ewing, R. P.; Sahimi, M. Tortuosity in Porous Media: A Critical Review. *Soil Sci. Soc. Am. J.* **2013**, *77*, 1461–1477. https://doi.org/10.2136/sssaj2012.0435.

(62) Ballard, A. L.; Sloan, E. D. The next Generation of Hydrate Prediction: I. Hydrate Standard States and Incorporation of Spectroscopy. *Fluid Phase Equilib.* **2002**, *194–197*, 371–383. https://doi.org/10.1016/S0378-3812(01)00697-5.

(63) Ballard, A. L.; Sloan, E. D. The next Generation of Hydrate Prediction: Part III. Gibbs Energy Minimization Formalism. *Fluid Phase Equilib.* **2004**, *218* (1), 15–31. https://doi.org/10.1016/j.fluid.2003.08.005.

(64) Jager, M. D.; Ballard, A. L.; Sloan, E. D. The next Generation of Hydrate Prediction: II.

Dedicated Aqueous Phase Fugacity Model for Hydrate Prediction. *Fluid Phase Equilib.* **2003**, *211* (1), 85–107. https://doi.org/10.1016/S0378-3812(03)00155-9.

(65) Ballard, A. L.; Sloan, E. D. The next Generation of Hydrate Prediction IV: A Comparison of Available Hydrate Prediction Programs. *Fluid Phase Equilib.* **2004**, *216* (2), 257–270. https://doi.org/10.1016/j.fluid.2003.11.004.

(66) Davies, J. T.; Rideal, E. K. *Interfacial Phenomena*, 1st ed.; Press, A., Ed.; Academic Press: New York, 1961.

(67) Rohatgi, A. Web Plot Digitizer 3.9. 2010.

(68) Palani, N.; Ramalingam, V.; Ramadoss, G.; Seeniraj, R. V. Study of Slip Velocity and Application of Drift-Flux Model to Slip Velocity in a Liquid–Solid Circulating Fluidized Bed. *Adv. Powder Technol.* **2011**, *22* (1), 77–85. https://doi.org/10.1016/j.apt.2010.03.016.

(69) Hinze, J. O. Fundamentals of the Hydrodynamic Mechanism of Splitting in Dispersion Processes. *AIChE J.* **1955**, *1* (3), 289–295. https://doi.org/10.1002/aic.690010303.

(70) Hughmark, G. A. Drop Breakup in Turbulent Pipe Flow. *AIChE J.* **1971**, *17* (4), 1000. https://doi.org/10.1002/aic.690170440.

(71) Kubie, J.; Gardner, G. C. Drop Sizes and Drop Dispersion in Straight Horizontal Tubes and in Helical Coils. *Chem. Eng. Sci.* **1977**, *32* (2), 195–202. https://doi.org/10.1016/0009-2509(77)80105-X.

(72) Karabelas, A. J. Droplet Size Spectra Generated in Turbulent Pipe Flow of Dilute Liquid/Liquid Dispersions. *AIChE J.* **1978**, *24* (2), 170–180. https://doi.org/10.1002/aic.690240203.

(73) Lovick, J.; Angeli, P. Droplet Size and Velocity Profiles in Liquid–Liquid Horizontal

Flows. *Chem. Eng. Sci.* **2004**, *59* (15), 3105–3115. https://doi.org/10.1016/j.ces.2004.04.035.

(74) Turner, D. J.; Miller, K. T.; Sloan, E. D. Direct Conversion of Water Droplets to Methane Hydrate in Crude Oil. *Chem. Eng. Sci.* **2009**, *64* (23), 5066–5072. https://doi.org/10.1016/j.ces.2009.08.013.

(75) InfoChem/KBC Advanced Technologies PLC, User Guide for Models and Physical Properties.

(76) Calsep, PVTsim Technical Overview http://www.calsep.com/uploads/Modules/Footerbrochure/technical.pdf.

(77) Vysniauskas, A.; Bishnoi, P. R. A Kinetic Study of Methane Hydrate Formation. *Chem. Eng. Sci.* **1983**, *38* (7), 1061–1072. https://doi.org/10.1016/0009-2509(83)80027-X.

(78) Vysniauskas, A.; Bishnoi, P. R. Kinetics of Ethane Hydrate Formation. *Chem. Eng. Sci.* **1985**, *40* (2), 299–303. https://doi.org/10.1016/0009-2509(85)80070-1.

(79) Turner, D. J. Clathrate Hydrate Formation in Water-in-Oil Dispersions, PhD Thesis, Colorado School of Mines, Golden/CO, United States, 2005.

(80) Rao, I. Multiphase Flow Modeling and Deposition of Hydrates in Oil and Gas Pipelines, PhD Thesis, Colorado School of Mines, Golden/CO, United States, 2013.

(81) Zerpa, L. E.; Rao, I.; Aman, Z. M.; Danielson, T. J.; Koh, C. A.; Sloan, E. D.; Sum, A. K. Multiphase Flow Modeling of Gas Hydrates with a Simple Hydrodynamic Slug Flow Model. *Chem. Eng. Sci.* **2013**, *99*, 298–304. https://doi.org/10.1016/j.ces.2013.06.016.

(82) Zerpa, L. E.; Sloan, E. D.; Sum, A. K.; Koh, C. A. Overview of CSMHyK: A Transient Hydrate Formation Model. *J. Pet. Sci. Eng.* **2012**, *98–99*, 122–129. https://doi.org/10.1016/J.PETROL.2012.08.017.

(83) Straume, E. O.; Morales, R. E. M.; Sum, A. K. Perspectives on Gas Hydrates Cold Flow Technology. *Energy & Fuels* **2019**, *33* (1), 1–15. https://doi.org/10.1021/acs.energyfuels.8b02816.

(84) Shi, B.; Liu, Y.; Ding, L.; Lv, X.; Gong, J. New Simulator for Gas–Hydrate Slurry Stratified Flow Based on the Hydrate Kinetic Growth Model. *J. Energy Resour. Technol.* **2018**, *141* (1), 012906. https://doi.org/10.1115/1.4040932.

(85) Bassani, C. L.; Pereira, F. H. G.; Barbuto, F. A. A.; Morales, R. E. M. Modeling the Scooping Phenomenon for the Heat Transfer in Liquid-Gas Horizontal Slug Flows. *Appl. Therm. Eng.* **2016**, *98*, 862–871. https://doi.org/10.1016/j.applthermaleng.2015.12.104.

(86) Bergman, T. L.; Lavine, A. S.; Incropera, F. P.; DeWitt, D. P. *Fundamentals of Heat and Mass Transfer*, 7th ed.; John Wiley & Sons Inc., 2011.

Supporting Information

1. Proof that heat transfer in capillary and particle-scales is negligible

Literature often considers that the exothermic nature of hydrate formation and related heat release once hydrates form cause a decrease in the driving force if ever the heat is not transferred from the growing surface. The heat transfer limitation was modeled in the pipeline length-scale[22,80,81,84] and in the micro-scale of interaction between particle and mixture bulk[14,21]. In this appendix, we show that the micro-scale heat transfer is not important in flowing systems, that is, the shear is always enough to equilibrate the temperature of the growing surface to the bulk one (in coherence with the observed by Sampaio et al.[21] that the particle-to-bulk temperature gradient is never higher than 0.2 K). This simplifies considerably the equations developed in section 2 of the article. Further consideration of heat transfer from the mixture to the outer medium/ocean (pipeline-scale) is dependent on multiphase flow convection and the pipeline material and thickness[22]. That is, the temperature of the growing surface is considered equal to the bulk temperature in means that the heat released by crystallization in one capillary or in one particle is instantly transferred to the bulk. However, *the bulk can change in temperature along time depending on the heat release rate of all particles; and the heat transfer rate of the flow to the pipeline wall and to the outer medium*. Coupling of the growth kinetic model with multiphase flow will be shown in the next parts of this series.

Figure S14 presents the heat transfer resistances from the outer surface of the particle to the external medium. The heat release due to growth of the outer surface and the capillary walls of one particle $\dot{Q}_{hyd,i}$ is transferred to the bulk through a heat transfer coefficient $h_{p/b}$. The mixture

changes heat with the internal wall through multiphase flow convection (Figure S14(b)) and the heat flux is due to heat release of the entire particle population $\dot{Q}_{hyd} = \sum_i \dot{Q}_{hyd,i} \approx n_p \dot{Q}_{hyd,i}$. Heat exchange between the mixture and the wall is especially attributed to the wetted perimeter of the gaseous and the pseudo-liquid phase[85] (slurry composed of water, oil and hydrate). The wall presents a heat transfer resistance due to conductivity (Figure S14(c)); and the external wall transfers heat with the external medium by convection (Figure S14(d)). The external medium temperature is usually the boundary condition of the problem (which is the ocean temperature).

The heat flux passing from one particle to the bulk is:

$$\dot{Q}_{hyd,i} = M_g \Delta h_{hyd} \left(-\left. \frac{dn_{g,i}}{dt} \right|_{hyd} \right) \tag{S44}$$

where Δh_{hyd} is the enthalpy of formation of gas hydrates expressed in J/mol of gas consumed. The thermal inertia due to the particle mass heating will not be considered (steady-state assumption). Furthermore, this model consider that the particles do not interact between themselves, only with the bulk (dilute flow hypothesis). Using Newton's law of cooling, the temperature difference between the particle and the bulk is:

$$\dot{Q}_{hyd,i} = M_g \Delta h_{hyd} \left(-\left. \frac{dn_{g,i}}{dt} \right|_{hyd} \right) = 4\pi r_p^2 h_{p/b} \left(T_{out} - T_b \right) \rightarrow \left(T_{out} - T_b \right) = \frac{M_g \Delta h_{hyd}}{4\pi r_p^2 h_{p/b}} \left(-\left. \frac{dn_{g,i}}{dt} \right|_{hyd} \right) \tag{S45}$$

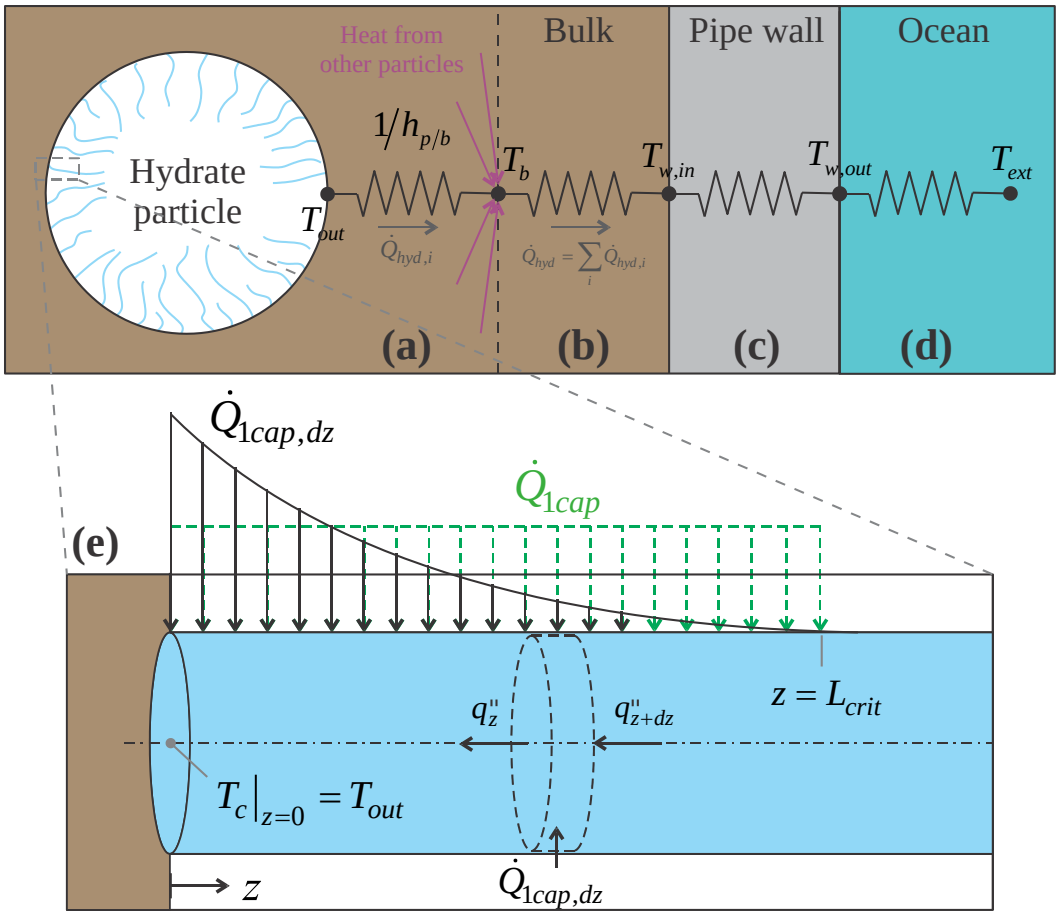

Figure S14. Depiction of heat transfer resistances associated to the system. (a) Convection between hydrate particle and bulk, being the heat transfer rate related to the heat release due to hydrate formation in one particle. (b) Convection between the bulk and the pipeline wall, being the heat transfer rate related to the heat release of the entire particles' population. (c) Conduction through the pipeline. (d) Convection between the pipeline outer wall and the external medium (the ocean). (e) Heat release due to crystallization in the capillary walls is diffused axially through the capillary.

Table S3 presents the closure parameters adopted, extra to the ones of mass transfer and crystallization already presented in Table S1 of the article. Equation (S45) gives $\left(T_{out} - T_b\right) < 0.4$ K

even if no-slip particle/bulk is considered (thus purely diffusive problem, with $\mathrm{Nu_p} = 2$) for $r_p = 1\,\mathrm{mm}$. This result is in agreement with Sampaio et al.[21]. For the case of turbulent flow and considering slip velocities of $U_{p/b} > 0.1\,\mathrm{m/s}$, then $\left(T_{out} - T_b\right) < 0.05\,\mathrm{K}$, which can be considered as thermal equilibrium. The temperature gradient $\left(T_{out} - T_b\right)$ is important only when larger particles are considered $(r_p > 5\,\mathrm{mm})$ and for creeping flow (low or non-existent slip), which is however not the case of oil and gas production.

Further heat release occurs in the capillary walls. Figure S14(e) depicts the heat generation distribution in the walls of one capillary $\dot{Q}_{1cap(z)}$ and the heat diffusion to the outer surface. Applying the energy balance, neglecting any convection, considering that the capillary wall is insulant (that is, all the heat transfer occurs only through water; although this is not well-posed, it implies in larger temperatures at the growing surface, thus able to prove our point that capillary and outer surface temperatures are practically the same), and adopting a constant thermal conductivity for the water k_w:

$$\frac{d}{dz}\left[-k_w \pi r_c^2 \frac{dT_c}{dz}\right] = \dot{Q}_{1cap,dz} \rightarrow \frac{d^2 T_c}{dz^2} + \frac{\dot{Q}_{1cap,dz}}{k_w \pi r_c^2} = 0 \tag{S46}$$

where T_c is the temperature at the capillary wall. The heat release per unit length of the capillary $\dot{Q}_{1cap,dz}$ is a function of the gas consumption in length dz inside of one capillary:

$$\dot{Q}_{1cap,dz} = \Delta h_{hyd}\left(-\left.\frac{dn_{g,i}}{dt}\right|_{1\,cap,dz}\right) \tag{S47}$$

and by using the crystallization law (Eq. (1) of the article):

$$-\left.\frac{dn_{g,i}}{dt}\right|_{1\,cap,dz} = 2\pi r_c^2 k_i f_{eq} \bar{C}_{(\bar{z})} d\bar{z} \tag{S48}$$

and the gas concentration distribution inside the capillary comes from Eq. (22) of the article. Substitution of Eq. (22) (of the article), Eqs. (S47) and (S48) in (S46) gives rise to a non-linear ODE. Therefore, $\dot{Q}_{1cap,dz}$ is assumed constant over the critical penetration length of gas inside the capillaries L_{crit}. The critical length is defined as the z value where $f|_{z=L_{crit}} \approx f_{eq}$. For values of $z > L_{crit}$, there is no heat release. Therefore, $\dot{Q}_{1cap,dz}$ is approximated as:

$$\dot{Q}_{1cap,dz} \approx \begin{cases} \dfrac{\dot{Q}_{1cap}}{L_{crit}} & \text{for} \quad 0 \le z \le L_{crit} \quad \text{with } \dot{Q}_{1cap} = \Delta h_{hyd} \left(-\left.\dfrac{dn_{g,i}}{dt}\right|_{1\,cap} \right) \\ 0 \quad \text{for} \quad z > L_{crit} \end{cases} \tag{S49}$$

where the gas consumption inside one capillary comes from $Ha_c L_{crit}/r_c \approx 2.5$ (discussion in section 2 of the article). The approximation of Eq. (S49) overestimate the temperature of the capillary walls, since the uniform distribution causes heat release deeper inside the capillaries. As already commented, an overestimation of T_c is not a problem since we want to prove that $T_c - T_{out} \to 0$.

The first boundary condition is a known temperature at the outer surface of the particle, Eq. (S7) . The second boundary condition considers that there is no heat transfer with the inner part of the particle (i.e., neglecting thermal inertia of the inner mass of the particle), Eq. (S8), evaluated at the critical penetration length.

$$T_c|_{z=0} = T_{out} \tag{S50}$$

$$\left.\frac{dT_c}{dz}\right|_{z=L_{crit}} = 0 \tag{S51}$$

Table S3. Closure parameters for heat transfer model, Eqs. (S45) and (S10) (other parameters come from Table 1 of the article).

Parameter	***Adopted value / correlation***
Heat transfer coefficient particle/bulk (Whitaker apud[86])	$\mathrm{Nu_p} = 2 + \left(0.4\,\mathrm{Re_p^{1/2}} + 0.06\,\mathrm{Re_p^{2/3}}\right)\mathrm{Pr_o^{2/5}}\left(\frac{\mu}{\mu_s}\right)^{1/4}$ [a]
Enthalpy of formation of CH_4 hydrates[55]	$\Delta h_{hyd} \approx 53$ kJ/mol of gas
Maximum gas consumption rate per particle	$-dn_{g,i}/dt\big\vert_{hyd,\max} \approx 4.8\times10^{-8}$ mol/s [b]
Maximum gas consumption rate per capillary	$-dn_{g,i}/dt\big\vert_{1cap,\max} \approx 5\times10^{-15}$ mol/s [c]
Critical penetration length	$L_{crit} = 2.5 r_c/\mathrm{Ha_c}$ [d]

[a]Valid for $0.71 \le \mathrm{Pr} \le 380$, $3.5 \le \mathrm{Re_p} \le 7.6\times10^4$ and $1.0 \le \mu/\mu_s \le 3.2$. With: $h_{p/b} = \mathrm{Nu_p} k_o/(2r_p)$; $\mathrm{Re_p} = 2\rho_o U_{p/b} r_p/\mu_o$; Pr_o is the Prandtl number of oil, considered equal to water ≈ 12; μ_s is the fluid viscosity in the surface temperature, considered the same as in the bulk, thus $(\mu/\mu_s)^{1/4} \approx 1$; k_o is the thermal conductivity of the oil, considered in the same order of magnitude of water ≈ 0.5 W/(m.K). [b]From the experiment (Figure 5 of the article), $-dn_g/dt\big\vert_{hyd,t=t_{nuc}} \approx 1.1\times10^{-3}$ mol/s. From Eq. (37) of the article, the number of particles is $n_p = 2.3\times10^4$ (for $r_p = 1$ mm). Considering even crystallization in all particles, then $-dn_{g,i}/dt\big\vert_{hyd,\max} = \left(-dn_g/dt\big\vert_{hyd,\max}\right) n_p^{-1}$. [c]Considering that $-dn_{g,i}/dt\big\vert_{1cap,\max} = \left(-dn_{g,i}/dt\big\vert_{hyd,\max}\right) n_c^{-1}$, where the number of capillaries per particle comes from Eq. (31) of the article, $n_c = 9.6\times10^6$, using the $\varepsilon_{in} = 60\%$ and $r_c = 500$ nm. [d]Hatta number is estimated through Eq. (14) of the article.

Solution of Eq. (S46) with Eqs. (S49), (S50) and (S51) gives:

$$T_c = T_{out} + \frac{\Delta h_{hyd}}{k_w \pi r_c^2}\left(-\left.\frac{dn_{g,i}}{dt}\right|_{1\,cap}\right)\left(z - \frac{z^2}{2L_{crit}}\right) \text{ for } 0 \le z \le L_{crit} \tag{S52}$$

where $T_c\big\vert_{z>L_{crit}} = T_c\big\vert_{z=L_{crit}}$, given the consideration of no thermal inertia of the inner mass of the particle. Therefore, the maximum temperature gradient between the capillary and the outer surface is at $z = L_{crit}$:

$$T_c^{\max} - T_{out} = T_c\big\vert_{z=L_{crit}} - T_{out} = \frac{L_{crit}\Delta h_{hyd}}{2k_w \pi r_c^2}\left(-\left.\frac{dn_{g,i}}{dt}\right|_{1\,cap}\right) \tag{S53}$$

From values of Table 1 (of the article) and Table S3, evaluation of Eq. (S53) gives $T_c^{\max} - T_{out} < 5\times10^{-3}$ K, which is a negligible temperature gradient. Even for the lower constant of crystal integration $k_i \approx 5.5\times10^{-12}$ mol/(m^{2}sPa) (i.e., deeper penetration of gas into capillaries), the smaller capillaries $r_c = 100$ nm and fair large particles $r_p = 10$ mm, the capillary/outer surface can be considered at thermal equilibrium, with $T_c^{\max} - T_{out} < 0.05$ K.

As a general conclusion for the scenarios considered (particles in the size-scale of mm; capillaries in the size scale of 100's of nm; k_i in the range of $10^{-12} - 10^{-7}$ mol/(m^{2}sPa); and highly agitated systems where slip velocity between particle and bulk is non-negligible), *the capillary walls, the outer surface of the particle and the mixture bulk can be considered at thermal equilibrium,* $T_c \approx T_{out} \approx T_b$.

2. Mathematic demonstrations

<u>Demonstration #1</u>: finding the linear outer growth rate of a particle dr_p/dt ***for application in Population Balance***

The linear growth of a surface relates to the gas consumption rate as:

$$\frac{dL}{dt} = \frac{1}{A}\frac{(\eta+1)}{(1-\varepsilon)}\frac{M_h}{\rho_h}\left(-\frac{dn_g}{dt}\right) \tag{S54}$$

where A is the growing surface area and ρ_h is the hydrate density of a perfect crystal (note that $(1-\varepsilon)\rho_h$ represents the density of the porous hydrates with empty pores). The 'molar mass of hydrates', M_h, is a fictitious parameter (since there is not such a 'mol of hydrates') and needs to be coherent with the 'stoichiometric relation' adopted, here considered as

$1G+\eta H_2O \rightarrow (\eta+1)Hyd$. Literature diverges when adopting this 'stoichiometric relation', where in some cases the multiplier of the 'mol of hydrates' is 1 instead of $(\eta+1)$. For the considered relation, $M_h = \left(M_g + \eta M_w\right)/(\eta+1)$, where M_g and M_w are the molar mass of gas and water. Using the expression of gas consumption due to outer growth $-dn_{g,i}/dt\big|_{out}$ (Eq. (11) of the article) in (S54) and applying to the outer surface of a spherical particle (i.e., $L = r_p$; $A = 4\pi r_p^2$):

$$\frac{dr_p}{dt} = \frac{1}{4\pi r_p^2}\frac{(\eta+1)}{(1-\varepsilon)}\frac{M_h}{\rho_h}\min\left\{\begin{array}{l}\zeta\dfrac{\pi}{3}\dfrac{\rho_w}{\eta M_w}\dfrac{r_c r_p}{\tau^2}\dfrac{\sigma_{o/w}\cos\theta_{o/w/h}}{\mu_w}\varepsilon\ ; \\ 4\pi r_p^2\dfrac{k_i}{H_o}\left[C_b - H_o f_{eq} - \dfrac{1}{4\pi r_p^2}\dfrac{1}{h_{m,p/b}}\left(-\dfrac{dn_{g,i}}{dt}\bigg|_{hyd}\right)\right]\end{array}\right\} \tag{S55}$$

which is an ODE that expresses the outer growth of a particle.

<u>Demonstration #2</u>: finding the gas consumption rate due to crystallization in capillary walls $-dn_g/dt\big|_{cap}$

The gas consumption rate over the extension of one capillary (*1cap*) of one particle *i* comes from the crystallization law, Eq. (1) of the article. Since the gas concentration varies along the capillary axial direction *z*, then integration along the entire capillary length L_c is needed, where the crystallization surface of an element *dz* equals $A = 2\pi r_c dz$ (cylindrical capillary):

$$-\frac{dn_{g,i}}{dt}\bigg|_{1\,cap} = \int_0^{L_c}\frac{k_i}{H_w}\left(C_{(z)} - H_w f_{eq}\right)2\pi r_c dz = \int_0^{\bar{z}_c} 2\pi r_c^2 k_i f_{eq}\bar{C}_{(\bar{z})}d\bar{z} \tag{S56}$$

where the capillary radius variation with z coordinate due to crystallization in the wall is neglected for mathematical simplification. Using the expression for gas concentration distribution inside the capillary (Eq. (22) of the article, where core shrinkage is neglected):

$$-\left.\frac{dn_{g,i}}{dt}\right|_{1\,cap} = \frac{2\pi r_c^2}{\mathrm{Ha_c}} k_i f_{eq} \bar{C}_{out,w} \text{ for } \mathrm{Ha_c}\bar{L}_c \geq 2.5 \tag{S57}$$

or yet returning to the primary variables:

$$-\left.\frac{dn_{g,i}}{dt}\right|_{1\,cap} = \pi r_c^{3/2} \sqrt{\frac{2D_w k_i}{H_w}} \left(C_{out,w} - H_w f_{eq}\right) \text{ for } \mathrm{Ha_c}\frac{L_c}{r_c} \geq 2.5 \tag{S58}$$

By: (i) substituting the expression of the gas concentration in the outer surface of the particle inside water $C_{out,w}$ (Eq. (10) of the article); (ii) recognizing that $-dn_{g,i}/dt\big|_{hyd} = -dn_{g,i}/dt\big|_{out} - n_c\, dn_{g,i}/dt\big|_{1cap}$; and (iii) multiplying by the number of capillaries per particle n_c and the number of particles in the system n_p; then (iv) the total gas consumption due to crystallization in the capillary walls comes:

$$-\left.\frac{dn_g}{dt}\right|_{cap} = n_p n_c \frac{\pi r_c^{3/2}}{(1+\omega)} \sqrt{2H_w D_w k_i} \left[\frac{C_b}{H_o} - f_{eq} - \frac{1}{4\pi r_p^2} \frac{1}{H_w h_{m,p/b}} \left(-\left.\frac{dn_{g,i}}{dt}\right|_{out}\right)\right] \tag{S59}$$

$$\omega = \frac{n_c}{h_{m,p/b}} \frac{H_w}{H_o} \frac{r_c^{3/2}}{4r_p^2} \sqrt{\frac{2D_w k_i}{H_w}} \tag{S60}$$

<u>Demonstration #3</u>: finding the maximum constriction rate of a capillary $-dr_c/dt\big|_{z=0}$

The volume variation of one capillary (*1cap*) in an element of length dz is related to the molar formation rate of hydrates by (see geometric parameters in Figure 4 of the article):

$$\left.\frac{dn_{h,i}}{dt}\right|_{1\,cap,dz} = -\frac{\rho_h}{M_h}\frac{d}{dt}\left(\pi r_c^2 dz\right) = \frac{\rho_h}{M_h} 2\pi r_c \left(-\frac{dr_c}{dt}\right) dz \tag{S61}$$

The hydrate formation rate is related to the gas consumption rate by the stoichiometric relation $1G + \eta H_2O \rightarrow (\eta+1)\,Hyd$:

$$\left.\frac{dn_{h,i}}{dt}\right|_{1\,cap,dz} = (\eta+1)\left(-\left.\frac{dn_{g,i}}{dt}\right|_{1\,cap,dz}\right) \tag{S62}$$

The gas consumption rate in a capillary element dz (with crystallizing surface $A = 2\pi r_c dz$, cylindrical capillary) comes from the crystallization law (Eq. (1) of the article):

$$\left.\frac{dn_{h,i}}{dt}\right|_{1\,cap,dz} = \frac{k_i}{H_w}\left(C_{(z)} - H_w f_{eq}\right) 2\pi r_c dz \tag{S63}$$

By combining Eqs. (S61) to (1):

$$-\frac{dr_{c(z)}}{dt} = (\eta+1)\frac{M_h}{\rho_h}\frac{k_i}{H_w}\left(C_{(z)} - H_w f_{eq}\right) = (\eta+1)\frac{M_h}{\rho_h}\frac{k_i}{H_w} H_w f_{eq} \bar{C}_{(z)} \tag{S64}$$

which is an expression for the constriction rate of the capillary in any z. The maximum constriction rate occurs at the maximum driving force, which is in the entrance of the capillary, $z = 0$. In this case, the driving force (gas concentration) comes from the boundary condition (Eq. (17) of the article; $C\big|_{z=0} = C_{out,w}$; which is related only to what is happening outside the capillary). The maximum constriction rate then comes:

$$-\left.\frac{dr_c}{dt}\right|_{z=0} = (\eta+1)\frac{M_h}{\rho_h}\frac{k_i}{H_w}\left(C_{out,w} - H_w f_{eq}\right) = (\eta+1)\frac{M_h}{\rho_h}\frac{k_i}{H_w} H_w f_{eq} \bar{C}_{out,w} \tag{S65}$$